FACHHOCHSCHULE AACHEN

ABTEILUNG JÜLICH

Fachbereich Physikalische Technik

Diplomarbeit

Klaus Schirmer

HERSTELLUNG VON SUPRALEITENDEN DÜNNEN V_3Si FILMEN DURCH D.C. MAGNETRON SPUTTERING

Referent FH Aachen: Prof. Dr. M. Müller-Veggian
Co-Referent INFN-LNL: Dr. V. Palmieri

Diese Arbeit wurde durchgeführt am
Istituto Nazionale di Fisica Nucleare
Laboratori Nazionali di Legnaro

Legnaro, Oktober 1999

Acknowledgements

This work was done under the scientific collaboration on superconductivity and thin films between Fachhochschule Aachen (Prof. Dr. M. Müller Veggian) and INFN (Dr. V. Palmieri). In Jülich Prof. Dr. M. J. Schöning substituted Dr. V. Palmieri for the final examination. This thesis was supported by the european Sokrates programm.

I would like to thank my supervisors, Prof. Dr. M. Müller-Veggian at FH Jülich and Dr. V. Palmieri at LNL for their support during my work.

Sincerest thanks are due to Walter Venturini and Dr. Yan Zhang for introducing me in most of the experimental techniques, for many interesting discussions and for their excellent support throughout the projekt.

I also wish to thank Renato Preciso for a lot of technical assistance and Giuseppina Grillo for her support and for her enormous patience.

Danksagung:

Diese Arbeit wurde im Rahmen der wissenschaftlichen Zusammenarbeit in dem Bereich Supraleitung und Dünnschichttechnik der Fachhochschule Aachen (Prof. Dr. M. Müller Veggian) und dem INFN (Dr. V. Palmieri). Für Dr. V. Palmieri übernahm in Jülich Prof. Dr. M. J. Schöning die Stelle des Zweitprüfers. Unterstützt wurde diese Diplomarbeit durch das europäische Sokrates-Programm.

Ich danke meinen Referenten, Prof. Dr. M. Müller Veggian an der FH Jülich und Dr. V. Palmieri am INFN für ihre Unterstützung während meiner Arbeit.

Besonderer Dank gilt Walter Venturini und Dr.Yan Zhang für die Einführung in die experimentellen Techniken, anregende Diskussionen und ihre ausgezeichnete Unterstützung bei der Durchführung der Arbeit.

Außerdem möchte ich Renato Preciso für die Anfertigung zahlreicher Bauteile der experimentellen Amaturen und Giuseppina Grillo für ihren Rücksichtnahme und ihre enorme Geduld bedanken.

Abbreviations:

λ : field penetration depth

α : ionization ratio per unit length

ω_0 : resonant frequency

A15 : crystal structure, also known as β-Wolfram structure

A_3B : binary compounds with a stoichiometry of 3:1

b : relativistic correction factor

BCS theory : theory of Bardeen, Cooper and Schrieffer, explaining the phenomenon of bounded electron pairs in superconductors

c : velocity of light

d : diameter of cavity cells from one iris to the next

DESY : Deutsches Elektronen Synchrotron, Hamburg

EBS : electron beam scattering

H_c : critical magnetic field

H_{c1} : lower critical magnetic field

H_{c2} : upper critical magnetic field

J_c : critical current

kT : kinetic temperature

LHC : Large Hadron Collider

P_d : dissipated power

Q_0 : quality factor

RBS : Rutherford backscattering

RRR : residual resistivity ratio

S : Bragg-Williams lattice order parameter

ST : Standard Theory

SZM : structure zone model

T_c : critical temperature

TESLA : TeV Energy Superconducting Linear Accelerator

TFTS : target-facing-type sputtering

T_m : melting temperature

TTF : Tesla Test Facility

V_s : bias potential

W_0 : energy stored in a resonator

Y : sputtering yield

1. Introduction

1.1 Preface 3

1.2 Radiofrequency Resonators 9

2. Materials

2.1 Fundamentals of superconductivity 12

2.2 Microscopic Theory 14

2.3 A15 materials 15

2.4 Phase diagram 17

3. Experimental Technique

3.1 The sputtering technique 18

3.2 The glow discharge 18

3.3 Diode sputtering 21

3.4 Magnetron sputtering 22

3.5 Thin film physical structure 24

3.6 Current-voltage relation 27

3.7 Double magnetron 28

3.8 Residual resistivity ratio RRR 33

3.9 System requirements 35

3.10 Measurement Technique 37

4. Sputtering Experiments

4.1 Configuration of the sputtering system 38

4.2 First V_3Si - Sputtering 39

4.3 Sputtering with a Substrate Heater 43

4.4 V_3Si Cosputtering without heating 47

4.5 V_3Si Cosputtering with heated substrate I 48

4.6 V_3Si Cosputtering with heated substrate II 49

5. Conclusions

50

6. References

51

1.1 Preface

TESLA is an acronym which stands for TeV Energy Superconducting Linear Accelerator.

Within the high energy physics community it is widespread consensus that an electron-positron linear collider with a center of mass energy of 500 to 1000 GeV and luminosity above $10^{33}cm^{-2}s^{-1}$ should be considered for top analyses and for reaching masses of more than 350 GeV.

Two complementary programmes are considered important: the realisation, in the ambit of international co-operation, of parts of a linear cryogenic accelerator of about 500 MeV installed at DESY, the study of new materials and the development of innovative technologies aimed at the abatement of production costs for high gradient cryogenic superconducting cavities, which are one of the critical elements for the future linear accelerators (this part of the programme was initially included in the superconducting special project).

The realisation of the test linear accelerator whose design energy was brought up to 1 GeV (Tesla Test Facility, TTF) has the objective of developing and completing the technology necessary for the realisation of an e+e- linear collider with an energy of 250+250 GeV (TESLA500) and a luminosity of $6 \cdot 10^{33}cm^{-2}s^{-1}$. In a later moment, the energy of this accelerator can be increased to 400+400 GeV (TESLA 800). The realisation of an accelerator with these features is complementary to the LHC as concerns the verification of ST, for example the precision studies of the properties of Higgs boson.

The TESLA approach to the 500 GeV collider is based on the use of superconducting (s.c.) accelerating structures . A test facility, located at DESY with major components flowing in from the members of the collaboration, is trying to establish a well-developed collider design. The facility includes infrastructure to prove the feasibility of accelerating gradients above 25 MV/m in a series production. The TESLA linear collider would rely on superconducting structures operating at 1.3 GHz with a gradient of 25 MV/m and an unloaded quality factor of $5 \cdot 10^{9}$ at T=2K.

Bulk Nb 9-cells cavities are currently prepared and succesfully tested.

However, Nb technology asks for superfluid He cooling systems. The use of a higher critical temperature superconductors would allow to adopt the simpler 4,2 K cryogenics.

V_3Si has a reported T_c value of 17 K , and RRR values up to 80.

1.1 Prefazione:

TESLA è un acronimo che sta per "TeV Energy Superconducting Linear Accelerator".

All'interno della comunità dei fisici delle alte energie c'è un consenso diffuso sulla oppurtunità di un collider lineare per elettroni-positroni con una energia nel riferimento del centro di massa di 500-1000 GeV e luminosità circa $10 \cdot 10^{34}$ cm-2s-1, per l'approfondimento delle tematiche legate alle verifiche del modello standard, al bosone di Higgs, alle supersimmetrie.

Accanto alla realizzazione, nell'ambito di una cooperazione internazionale, dei componenti di un acceleratore lineare da 500 MeV, è in atto un programma di studio di nuovi materiali e di sviluppo tecnologico mirato all'abbattimento dei costi per le cavità superconduttrici ad alto gradiente, che sono uno degli elementi critici per i futuri acceleratori lineari.

La realizzazione di un acceleratore lineare di prova il cui progetto è stato spinto ad 1 GeV.

(TESLA Test Facility, TTF), ha lo scopo di sviluppare ed affinare la tecnologia necessaria a realizzare un collider lineare per elettroni e positroni con energia 250+250 GeV (TESLA 500) e luminosità $6 \cdot 10^{33}$cm-2s-1. Successivamente, l'energia di questa macchina potrà essere portata a 400+400 GeV (TESLA 800). Un tale acceleratore sarà complementare ad LHC per quanto concerne le verifiche del modello standard, per esempio gli eventuali studi sulle proprietà del bosone di Higgs.

L'approccio di TESLA ad un collider da 500 GeV è basato sull'uso di strutture acceleranti superconduttive. In un impianto test, situato a DESY, i cui componenti principali provengono dai membri della collaborazione, si sta procedendo a stabilire il progetto avanzato del collider. L'impianto comprende infrastrutture per verificare la fattibilità di campi acceleranti di 25 MV/m in una produzione in serie. TESLA dovrà fondarsi su cavità superconduttrici funzionanti a 1.3 GHz, con campo accelerante di 25 MV/m e fattore di merito Q "unloaded" $5 \cdot 10^9$ a T=2K.

Cavità a 9 celle in niobio massiccio vengono ordinariamente preparate e superano i valori di progetto prefissati.

Tuttavia, la tecnologia del niobio richiede l'uso di sistemi di refrigerazione con elio superfluido. L'impiego di un superconduttore con temperatura critica più alta consentirebbedi adottare sistemi a 4,2 K, più semplici ed economici.

Il composto V_3Si, oggetto di questa tesi, ha una temperatura critica, riportata in letteratura, di 17 K, con valori del rapporto di resistività RRR che raggiungono 80.

1.1 Einleitung

TESLA ist ein Akronym für „TeV Energy Superconducting Linear Accelerator“.
Unter den Hochenergiephysikern herrscht eine weitreichende Übereinstimmung, daß ein Elektron-Positron-Collider mit einer Mittelpunktsenergie von 500 bis 1000 GeV und einer Luminosität von über 10^{33} $cm^{-2}s^{-1}$ für Top-Analysen und zum Erreichen von Massen von mehr als 350 GeV in Betracht gezogen werden sollte.
Zwei ergänzende Programme werden hierfür als wichtig erachtet:
- die Realisierung, im Bereich einer internationalen Zusammenarbeit, von Teilen eines cryogenen Linearbeschleunigers von etwa 500 MeV aufgebaut bei DESY
- die Untersuchung neuer Materialien und die Entwicklung inovativer Technologien mit der Vorgabe, die Produktionskosten für die supraleitenden cryogenen high gradient Cavities zu verringern. Diese sind die kritischen Elemente der zukünftigen Linearbeschleunigern (dieser Teil des Programms war anfänglich im „Superconducting Special Project“ enthalten).

Die Verwirklichung des Testlinearbeschleunigers, dessen angestrebte Energie auf 1 GeV herraufgesetzt wurde (Tesla Test Facility, TTF), hat das Ziel, die für Realisierung eines e+e- Linear Colliders mit einer Energie von 250+250 GeV (TESLA500) und einer Luminosität von $6 \cdot 10^{33} cm^{-2}s^{-1}$ notwendige Technik zu entwickeln und zu fertigen. Zu einem späteren Zeitpunkt kann die Energie dieses Beschleunigers auf 400+400 GeV (TESLA800) erhöht werden. Die Fertigstellung eines Beschleunigers mit diesen Eigenschaften wäre eine Ergänzung zu dem LHC (Large Hadron Collider) in Bezug auf die Bestätigung des Standardmodels, z.B. genauer Untersuchungen der Eigenschaften der Higgs Bosonen.

Die Annäherung von TESLA an einen 500 GeV Collider basiert auf der Verwendung von supraleitenden (superconducting = s.c.) Beschleunigerelementen. Eine Versuchsanlage bei DESY mit den Hauptelementen der an dem Gemeinschaftsprojekt beteiligten Mitglieder versucht den hochentwickelten Collider einzurichten. Diese Anlage beinhaltet die Infrastruktur zur Überprüfung der Machbarkeit von Beschleunigungsgradienten oberhalb von 25 MV/m in der Serienfertigung. Der TESLA Linear Collider würde auf

supraleitenden Strukturen basieren, die bei 1,3 GHz mit einem Gradienten von 25 MV/m betrieben werden und einen „unloaded" Qualitätsfaktor von $5 \cdot 10^9$ bei $T = 2$ K aufweisen.
Massive neunzellige Niob-Resonatoren werden gegenwärtig produziert und erfolgreich getestet.
Die Nb Technologie erfordert jedoch ein Kühlsystem unter Verwendung von suprаflüssigem Helium. Die Gebrauch von Supraleitern mit einer höheren kritischen Temperatur würde die Anwendung einer einfacheren und kostengünstigeren 4,2 K Kühlung erlauben.
Für die Binärlegierung V_3Si, dem Gegenstand dieser Diplomarbeit, sind in der Literatur kritische Temperaturen von 17 K belegt, wobei RRR-Werte von bis zu 80 erreicht wurden[30].

1.2 Radiofrequency Resonators

Each accelerator consists of rf accelerating structures and magnets to guide and focus the particle beam. The accelerating structures are composed of resonating cavities, which are energy storage devices employed for the radiofrequency and microwave range. The working principle is equivalent to a classical RLC resonant circuit[1]. The electromagnetic energy oscillates back and forth from entirely electric to entirely magnetic form of energy. The RLC circuit will resonate at a frequency $\omega = 1/\sqrt{LC}$. To make the circuit resonating at higher frequencies, a possibility is to decrease L as much as possible.

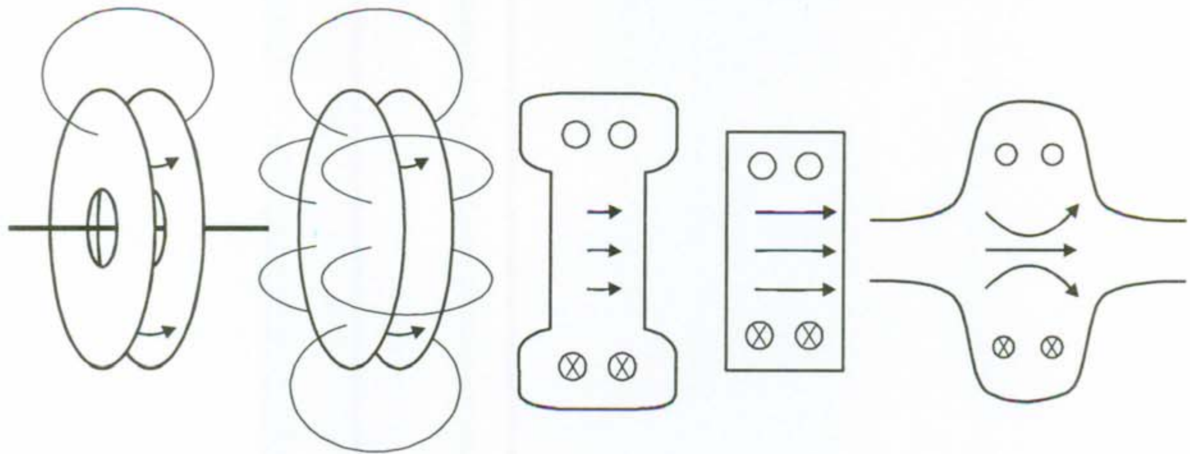

Fig. 1.1: Transformation of a L-C circuit into an accelerating cavity[2]

Inside the cavities different resonances can be excited, as shown in **fig. 1.1**, for accelerating cavities usually the TM_{010} mode is chosen. This mode has a longitudinal electric field along the cavity axis, which is surrounded by the circular field lines of the magnetic field. For highly relativistic particles such as electrons and positrons several cavitiy cells can be mounted in series. Each cell in this system must be coupled with the following.

The favourite coupling mode of accelerating structures is the so called π-mode, represented in **fig. 1.2** and **1.3**.

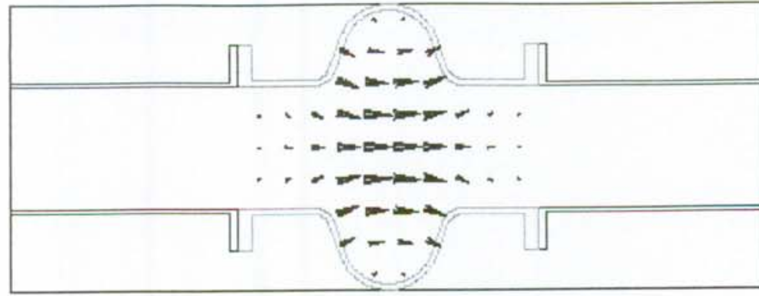

Fig. 1.2a: ***Fundmental TM_{010} mode electric field distribution***

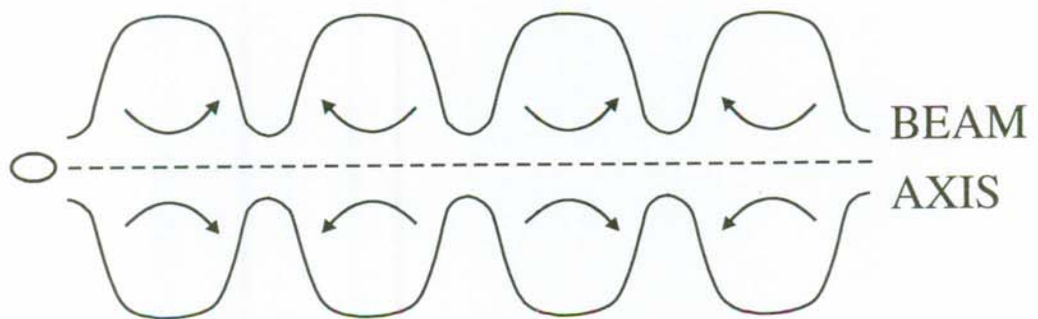

Fig. 1.2b: ***A multi-cell cavity excitied in the π-mode. This mode is characterised by the fact that accelerating fields in each pair of the cavities are equal in magnitude and opposite in direction.***

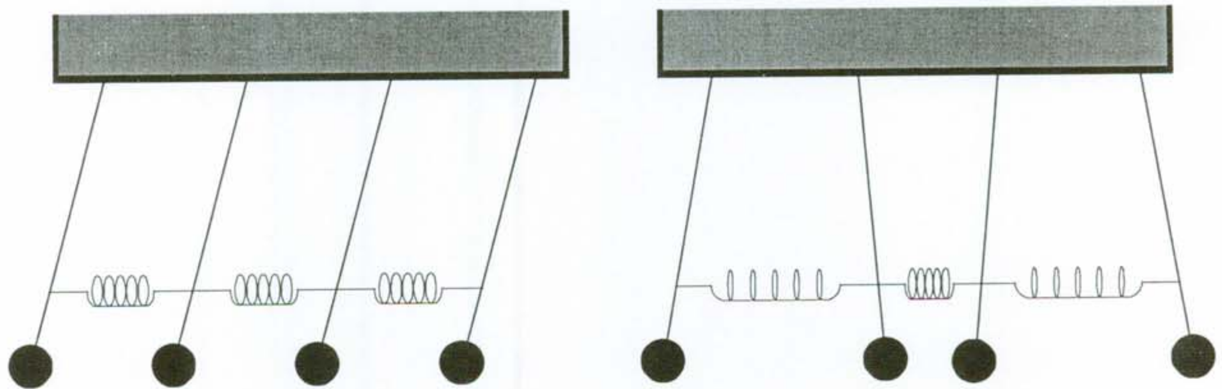

Fig. 1.3: ***The coupled pendula analogue[1]***
a) The zero-mode: The phase difference is zero
b) The Π-mode: The phase difference is Π

If the velocity of the particle bunch is synchronised with the frequency and phase of the rf fields in the cavity the bunch will be accelerated in each cell: In the first cell the field is parallel to the bunch, in the second cell it is antiparallel,

but it becomes parallel one semi-cycle later just when the beam arrives. To be accelerated in every cycle the particles velocity has to be adjusted to the effective electric length $v = b \cdot c$ and to the resonantfrequency f_0. This leads to the condition

$$d \cdot \omega_0 \leq \pi \cdot b \cdot c \tag{1.1}$$

That means that resonant frequencies for electron cavities range ($b \approx 1$) between 350 and 3000 MHz since d has values generally between 5 and 10 cm.

Independently of which resonance is excited inside the cavity, the field oscillation will get damped, if the cavity is left in free oscillation. This is caused by the non perfect conductivity of the resonators walls and by the losses through resonators ports, if present.

So energy initially stored into the cavity will exponentially decay with a damping time proportional to the quality factor Q_0.

$$W_{(t)} = W_0 \cdot e^{-(W_0/Q_0 \cdot t)} \tag{1.2}$$

The quality factor can be defined as

$$Q_0 = \omega_0 \cdot W/P_d \tag{1.3}$$

where W is the energy stored in the cavity, P_d the dissipated power and ω_0 the resonant frequency[3]. Since the energy leakage and also the frequency selectivity is proportional to the quality factor the ultimate Q is desired.

The quantity of the highest interest for particle physicists of course is the accelerating fields that can be obtained in the cavity. Higher accelerating fields allow a greater acceleration, i.e. a higher particle energy within a given structure length. Vice versa high fields allow to build acceleration structures of a shorter length, which results in much lower costs.

The Tesla collaboration has chosen a nine cell cavity with a resonance frequency of 1300 MHz. A Q_0 better than $5 \cdot 10^9$ at a accelerating field of 25 MV/m is required[4].

2. Materials

2.1 Fundamentals of superconductivity

Three years after the first liquefaction of helium in 1911, *Heike Kammerling-Onnes*(3) discovered that mercury completely lose its resistivity at temperatures below 4.15K. Today many other elements and compounds are known as superconductors. Decay time measurements of a current into a superconducting ring(5) prove that the resistivity of a superconductor is below 10^{-27} Ω/cm. So one can indeed speak of a total vanishing of electrical resistivity. The abrupt vanishing of resistance at a certain temperature in super-conductors is a phase transition into another state. The temperature T_s at which this phenomenon occurs is the critical temperature T_c. The element with the highest transition temperature is niobium (9.26K), and for many years the compound with the highest T_c has been a niobium-based one (Nb_3Ge, T_c = 23.2K). The discovery of a new class of superconducting materials by *Bednorz* and *Müller*(6) made it possible to find a compound with a T_c higher than the boiling point of nitrogen.

Compound	T_c [K]	Compound	T_c [K]
Nb_3Sn	18.05	$Pb_{0.7}Bi_{0.3}$	8.45
Nb_3Ge	22.3	V_3Si	17.1
NbN	16	$(SN)_x$	0.26
NbO	1.2	$(BEDT)_2Cu(NCS)_2$	10
$BaPb_{0.75}Bi_{0.25}O_3$	11	$La_{1.8}Sr_{0.2}CuO_4$	38
Ube_{13}	0.75	$Bi_2CaSr_2Cu_2O_{8+x}$	90

Table 2.1: ***Critical temperatures of some elements and compounds*** (7)

The absence of any resistance is the best known property of super-conductors, but there are also some other remarkable characteristics. In 1933, *Meissner* and *Ochsenfeld*(8) found that magnetic fields are squeezed out of a superconductor at temperatures below T_c. In normal materials there appears a finite induction B given by B=μH, when a magnetic field is applied. In diamagnetics (μ<1), the applied field is weakened and the induction B becomes smaller than H. In superconductors the magnetic permeability is zero, corresponding to ideal diamagnetism. This effect is due to electric currents induced in a thin surface

layer, in which the magnetic field penetrates. The magnetic field of these electric currents opposes the applied field: the result is zero magnetic induction inside the sample. The field penetration depth "λ" is one of the main characteristics of a superconductor. Its value is usually in the range of a few hundreds Ångstroms. If the magnetic field increases at some certain value, called critical field, it destroys superconductivity and the sample returns to the normal state. At zero temperature the critical field has a maximum, while at $T=T_c$ the critical field is zero. Its behavior can be approximately given by the formula

$$H_C(T) = H_{CO}(1-T/T_c)^2 \qquad (2.1)$$

where H_{CO} is the value of the critical field at zero temperature. Depending on the particular superconductor, the critical field can assume values in a rather wide range, but its existence is an universal feature for all superconducting materials.

Besides magnetic field and temperature, also current density can't exceed a given value if the superconducting state has to be maintained. Anyhow, unlike T_c and H_c, the critical current J_c strongly depends on the metallurgical history of the material, and so it varies from one sample to another. The properties so far outlined are typical of the so called "Type I superconductors". This type shows a sharp transition from the superconducting to the normal state for values less than T_c. Higher critical fields are provided by "Type II superconductors". This class of superconductors is different in regard to their magnetic behavior. Contrary to Type I superconductors they have two critical fields: H_{C1}, below which the material is entirely superconducting and an upper critical field H_{C2}, over which the sample is completely normal conducting. Between these two fields, the magnetic flux penetrates partially in the material, which is divided in normal conducting filaments called fluxoids, immersed in the superconducting phase.

2.2 Microscopic Theory

A systematic theory of superconductivity, which explained the nature of this phenomenon, was formulated in 1957 by ***Bardeen***, ***Cooper*** and ***Schrieffer***[9]. It based on a "condensation" of electrons into Cooper pairs. One basic result of the **BCS** theory is the presence of a forbidden energy gap delta in the energy spectrum of a superconductor. The gap of the order of kT_c is centered around the Fermi energy. For a critical temperature around 10 K kT_c is about 1 MeV. The gap is due to an attractive interaction between two electrons at energies close to the Fermi energy. Such interaction leads to a forming of bounded pairs, each of them composed by electrons of opposed spins and opposed moments. At the absolute zero all electrons are coupled in Cooper pairs, increasing the temperature, electron pairs start to depair and fill the energy levels above the gap. Electrical resistance in normal metals is connected to the scattering of electrons by impurities or the vibrations of the crystal lattice. Cooper pairs, in comparison, do not interact with the crystal lattice vibrations. As a result, they can move without friction.

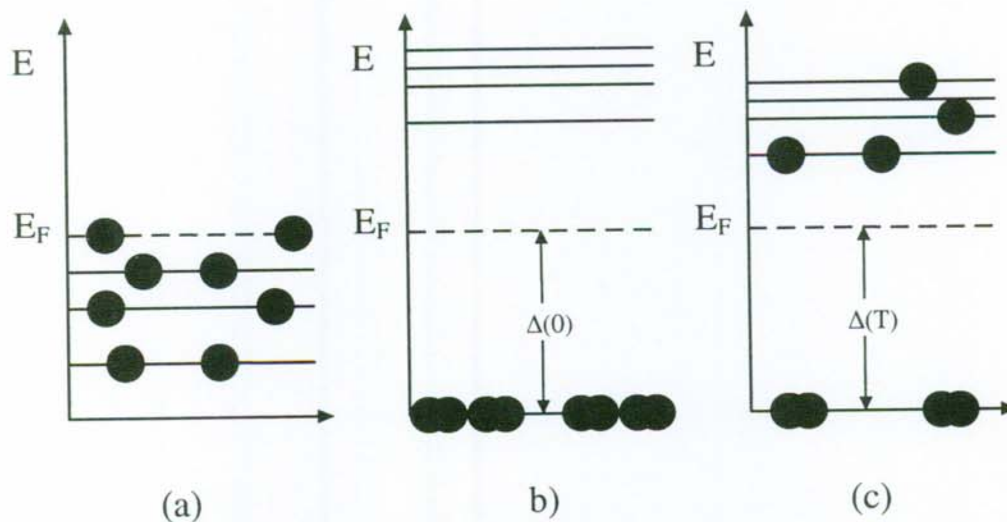

Fig. 2.1: Energyspectrum[10] for a) a normal metal b) a superconductor at T=0K c) a superconductor at T ≠0K

2.3 A15 materials

Before the discovery of the high-T_c oxide superconductors by *Bednorz* and *Müller* (1986), only compounds forming the A15 type structure were known to exhibit T_c values above 20K[10]. The stoichiometry of the A15-materials is A_3B. The B-atoms form a body centered cubic lattice, and the A-atoms are arranged by pairs on the cube edges, parallel to the coordinate axes.

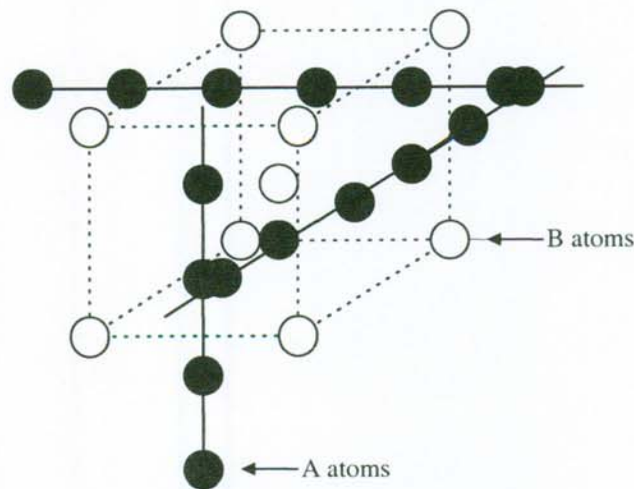

Fig. 2.2: ***crystal structure of A15- compounds***[7]

A typical feature of this structure is, that A atoms make up families of intersecting linear chains. The distance between the atoms within one chain being the shortest distance between the atoms in the A15 structure and being 22% less than that between A atoms belonging to different chains. The A atom is always a transition metal of groups IV, V or VI (Ti, V, Cr, Zr, Nb, Mo, Ta, W), while the B atom can be either a nontransition metal or a transition metal. From the phase diagrams of 28 compounds with A15 structure the A_3B compounds may be divided into two groups, according to how their regions of homogeneity are formed. The first group comprises compounds whose region of homogeneity is practically absent or extends only in the direction rich in the A component (V_3Si, V_3Ge, V_3Ga, V_3Au, Nb_3Ga, Nb_3Ge etc.). They are called "***typical***" by convention. In "*typical*" A15 the maximum values of T_c are obtained near the stoichiometric composition and at a high degree of order. Such situation is thought to be associated with the conservation of the integrity

of the linear chains in the A15 structure. The other group of compounds, which are called "***atypical***", contains compounds whose region of homogeneity extends towards the B component or in both directions from the stoichiometrical composition (Mo_3Ir, Mo_3Pt, Cr_3Os, V_3Ir etc.). In these compounds (having lower T_c) atoms in the chains are likely to be replaced by the B atoms and integrity is not conserved. In **table 2.3** data on superconducting transition temperatures in compounds with A15 structure are presented.

B\\A	Ti	Zr	Hf	V	Nb	Ta	Cr	Mo
Al				11.70	18.80			0.58
Ga				15.9	20.3		<0.35	0.76
In				13.9	8.8 - 9.2			
Tl	<0.35	<0.35		<4.20				
Si				17.1	18.0-19.0		<0.015	1.70
Ge				11.2	23.2	8.0	1.20	1.8
Sn	5.80	0.93		12.3-17.9	18.0	8.35		
Pb		0.76		<4.2	8.0			
P				<1.00				
As				0.20				
Sb	6.5	<1.20		0.80	2.0	0.72		
Bi		3.4		<4.20	3.0			

Table 2.3: ***T_c in compounds with A15 structure***[12]

This table shows, that the highest T_c for A_3B compounds of Vanadium and Niobium are obtained in those cases when the B atom is represented by a non transition element Al, Si, Ga, Ge, Sn. At deviations from stoichiometry and with the degree of long-range order S (the *Bragg-Williams order parameter* **S** is defined in such a way that S=1 for the perfectly ordered lattice and S=0 for complete disordering or random distribution) one can see, that T_c is very sensitive to these effects. For example, in the compound V_3Si of stoichiometric composition T_c varies from 16.85 to 17.1K, whereas at 20.1at.% Si T_c is 9.4K.[13]

2.4 Phase diagram

The knowledge of the precise limits of stability of the A15 phase is very important since the superconducting and normal state properties of many of the interesting systems depend critically on composition. If in a binary system an A15 phase occurs, this phase always immediately follows bcc solid solution with increasing concentration of the B component. On the higher concentration side, the A15 phase is often followed by phases exhibiting the tetragonal sigma structure (e.g. Nb-Ge). Among the A15 compounds with a $T_c > 15K$ there are only V_3Ga, V_3Si, and Nb_3Sn which are stable at the stoichiometric composition, whereas Nb_3Al, Nb_3Ge and Nb_3Ga are metastable and can only be produced with an excess of Niobium.

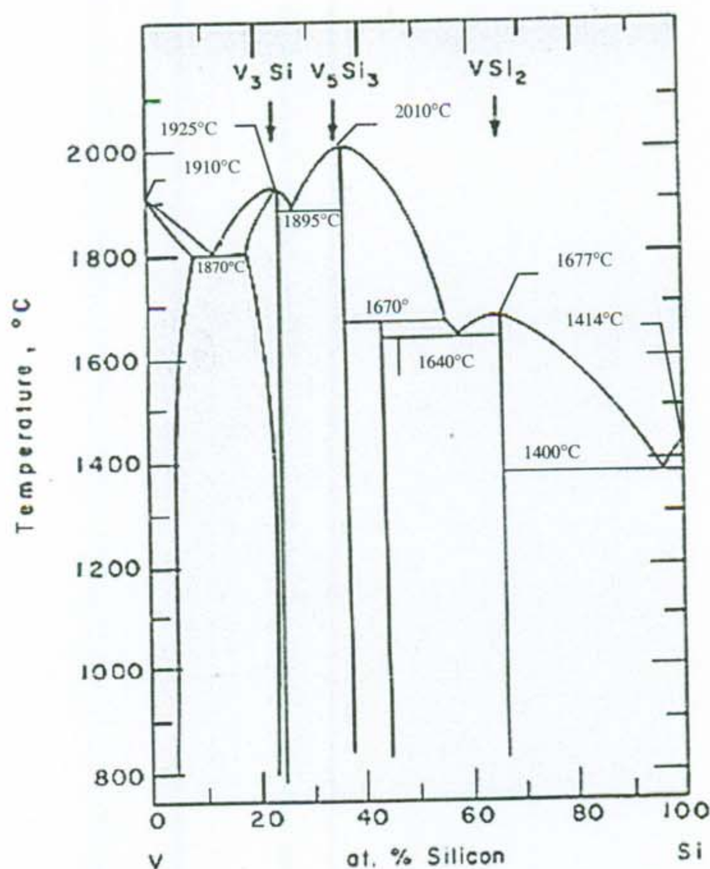

Fig. 2.3: *Phase diagram of V_3Si*[14]

3. Experimental Technique

3.1 The sputtering technique

Sputtering is the mechanically outknocking of atoms or molecules from the surface of a target by energetic ions. It is well-suited for the deposition of films of refractory metals, multi component alloys and compounds. The preparation of thin films by sputtering involves the transport of a material at the vapor phase from a source to a substrate. The ejection of source material into the vapor phase is accomplished by bombarding the surface of the source (target) with ions of sufficient energy, based on the phenomenon of a self-sustained glow discharge. The target surface disintegrates primarily as a result of momentum transfer between the incident ions and the target. The target ejected particles traverse the vacuum chamber and are subsequently condensed on a substrate to form a thin film.

3.2 The glow discharge

If a dc voltage is applied between two electrodes with the distance d in a gas at low pressure $10^{-2}-10^{-1}$ mbar, a small current will flow between the electrodes. It is caused by a small number of ions and electrons, which always exists in a gas due to ionization by cosmic radiation. With increasing the voltage, the electrons reach energies which enable them to ionize atoms by collision, each ionization process produces further electrons. The ions, that result from these collisions, are also accelerated by the applied field and move toward the cathode. When striking the cathode they can release secondary electrons. The secondary electron emission ratio of most materials is of the order of 0.1, so that several ions must bombard a given area of the cathode to produce another secondary electron. Initially, the bombardment is concentrated near the edges of the cathode. As more power is supplied, the bombardment covers the whole surface and a constant current is achieved. Further increase in power produces both increased voltage and current in a region known as the abnormal glow discharge. This mode is usually used in sputter deposition techniques. The two processes of ionization by electron impact and secondary emission of electron by ions thus control the current I in the system. If each electron, according to

the Townsend criterion

$$y \cdot e^{(\alpha \cdot d - 1)} = 1 \tag{3.1}$$

produce at least one new electron, the glow discharge burns self sustained (where *y* is the number of secondary electrons emitted per incident ion, α is the number of ions per unit length produced by the electrons and *d* is the spacing between the electrodes). This happens by the breakdown voltage, which is a function of the product of the pressure p and the electrode distance d (Paschen law). Within a glow discharge there exists distribution of potential, field, space charge and current density. Visually these are seen as regions of varied luminosity, as shown in **fig. 3.1**.

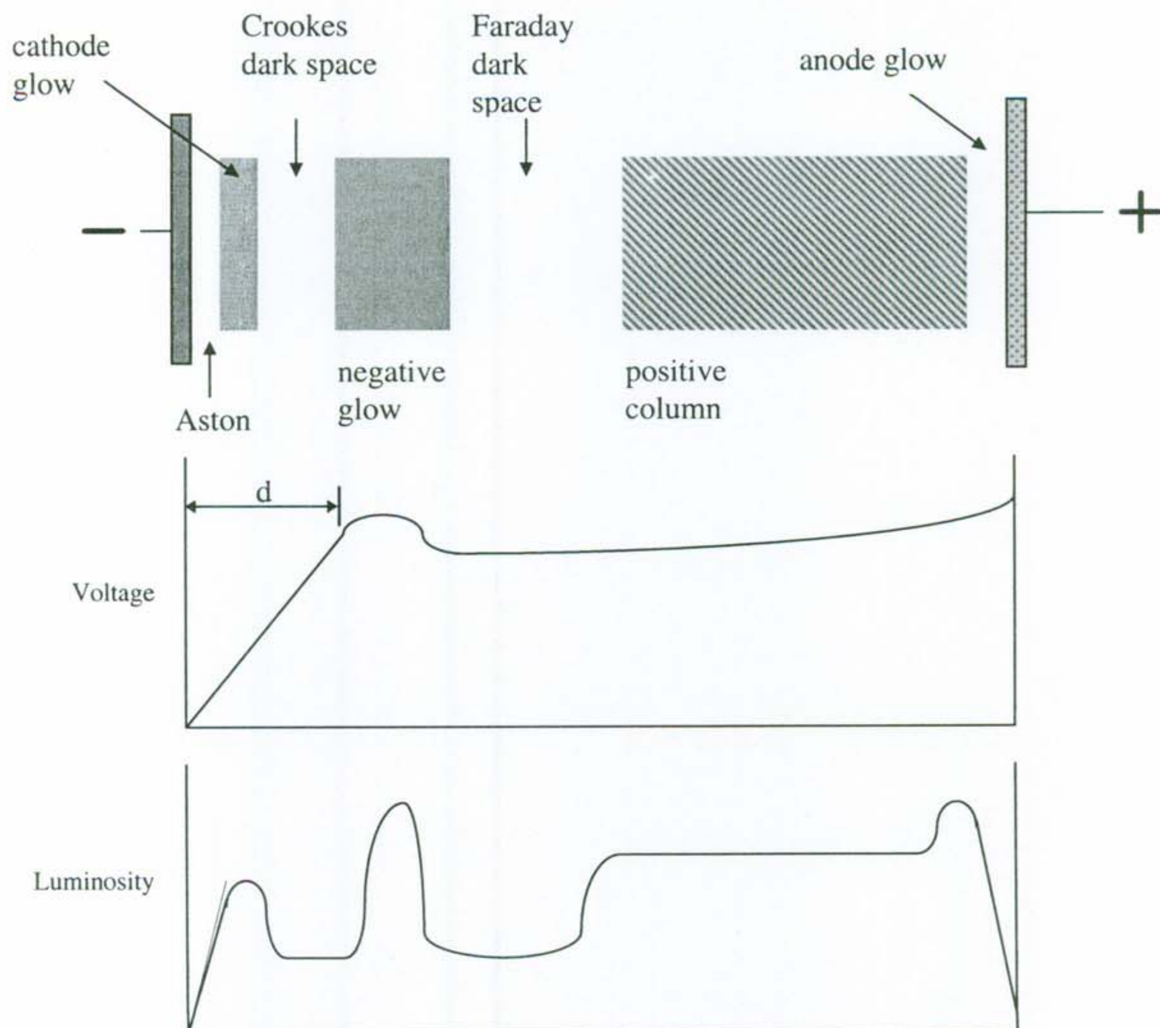

Fig. 3.1: ***Appearence of glow discharge at low pressure*** [15]

The various luminous and dark regions of a glow discharge arise in the following manner: electrons usually leave the cathode with a small velocity, the energy is of the order of one electron volt. They are not able to ionize gas molecules until they are accelerated to sufficient energies. This results in a region called "Aston's dark space". The cathode glow is the region in which the electrons reach energies corresponding to the ionization potential, and this is the luminous region closest to the cathode. In the "Crookes' dark space", the electron energies are over the maximum excitation potential, so that no visible light is emitted. When the negative glow is reached, the number of slow electrons (i.e. those produced by an ionizing collision) has become very large. These electrons do not have sufficient energy to produce ionization, but they do possess enough energy to cause excitation and are the cause of the negative glow. The "Faraday dark space" and the positive column are nearly field-free regions and are characterized by nearly equivalent numbers of ions and electrons. For glow discharges applied as sputtering sources, the electrode separation needs to be small so that the anode is located in the negative glow. Therefore, the positive column and the Faraday dark space does not exist.

3.3 Diode sputtering

The simplest configuration of a sputtering source is the diode sputtering configuration (**fig. 3.2**). It consists of a vacuum chamber in which between two electrodes an anomalous glow discharge will be created. The negative electrode (cathode) constitutes the target, whereas the substrate is placed on the anode. After evacuation to high vacuum the chamber is filled with the sputtering gas, usually argon, at a pressure of 10^{-2}-10^{-1} mbar. The discharge is created by applying a dc voltage of 1-5 kV between cathode and anode. The argon gas atoms will be ionized and accelerated towards the cathode, where they extract atoms from the target surface. The sputtered atoms diffuse in the chamber and finally condense on a surface. The kinetic energy of the atoms released is a few eV, i.e. substantially higher than that of evaporated atoms (kT=0.1eV at 1200K). These higher energies lead to a better adhesion and a higher density of the film. Almost every material can be sputtered, independent of the melting point or other physical properties. The number of released atoms per impinging ion is called the sputtering yield.

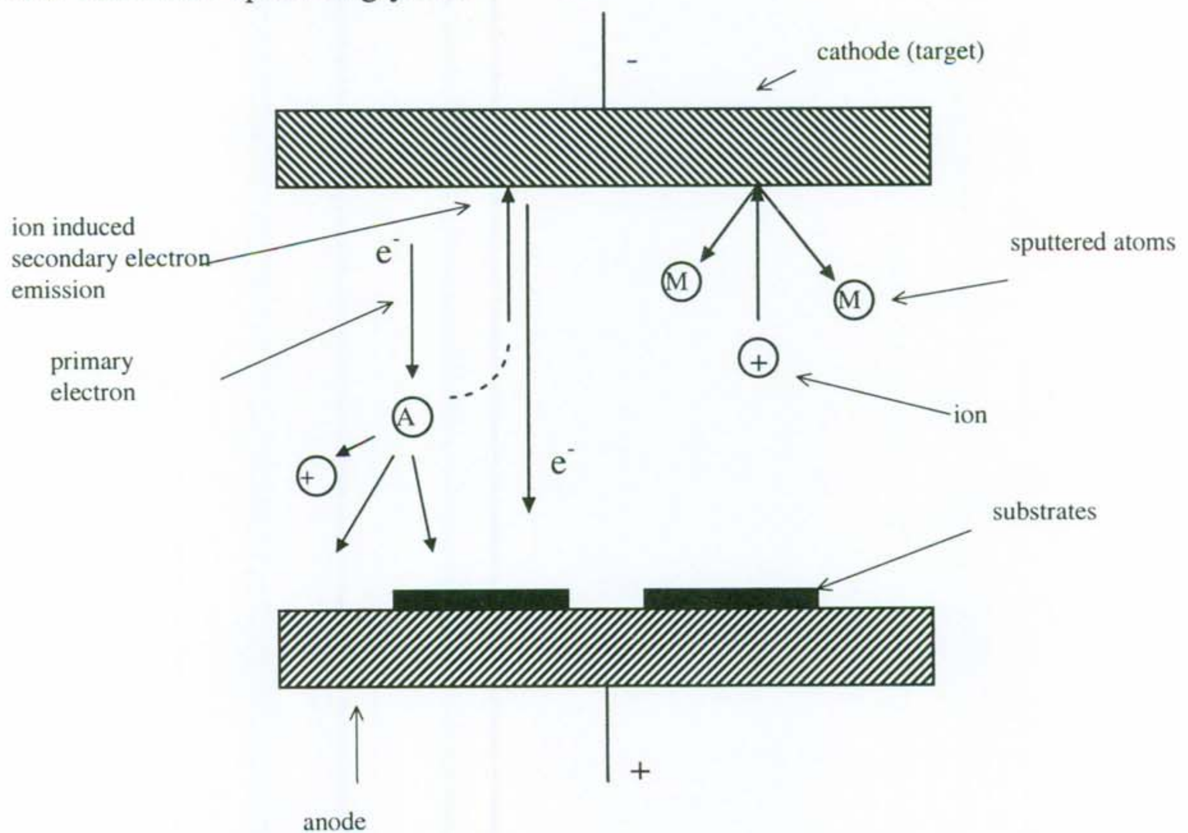

Fig. 3.2: ***schematic presentation of a diode sputtering source*** [16]

The sputtering yield depends on the following parameters:

Material: The yield Y is by a given species and energy of the ions reciprocal to the sublimation enthalpy of the target material(Y/E_0).[17]

Energy: The sputtering process starts at a threshold energy E_{thres} of 10-30 eV, and increasing linear with increasing ion energy. At energies from 10^4eV the sputtering yield reaches a bride maximum and after that it decreases because of ion implantation effects.[18]

Ion mass: The variation of the ion species at constant energies shows, that the sputtering yield has a maximum, when the ion mass M_i is approximately equal to the mass of the target atoms M_t.[19]

Incident angle: The sputtering yield increases with a growing incident angle Ω proportional to the cos Ω^{-1} law due to the smaller change of impulse by greater angles. With values of Ω near 90° the effect of ion reflection becomes dominant and Y decreases.[20]

3.4 Magnetron sputtering

For quite a few applications, sputter deposition rates of a few angstrom per second are not considered to be fast enough, either for economic reasons or for film structure reasons. For these applications, a higher rate sputter deposition process is required, and this is available through the use of magnetically enhanced plasma discharges generally known as magnetron discharges.

Magnetron sputtering sources can be defined as diode devices, in which magnetic fields are used to increase the distance the electrons have to travel by the forming of *electron traps*, thus increasing the probability of collision. Magnetic fields are used in concert with the cathode surface to form electron traps which are so configured that the $\vec{E} \times \vec{B}$ electron drift currents close upon themselves.

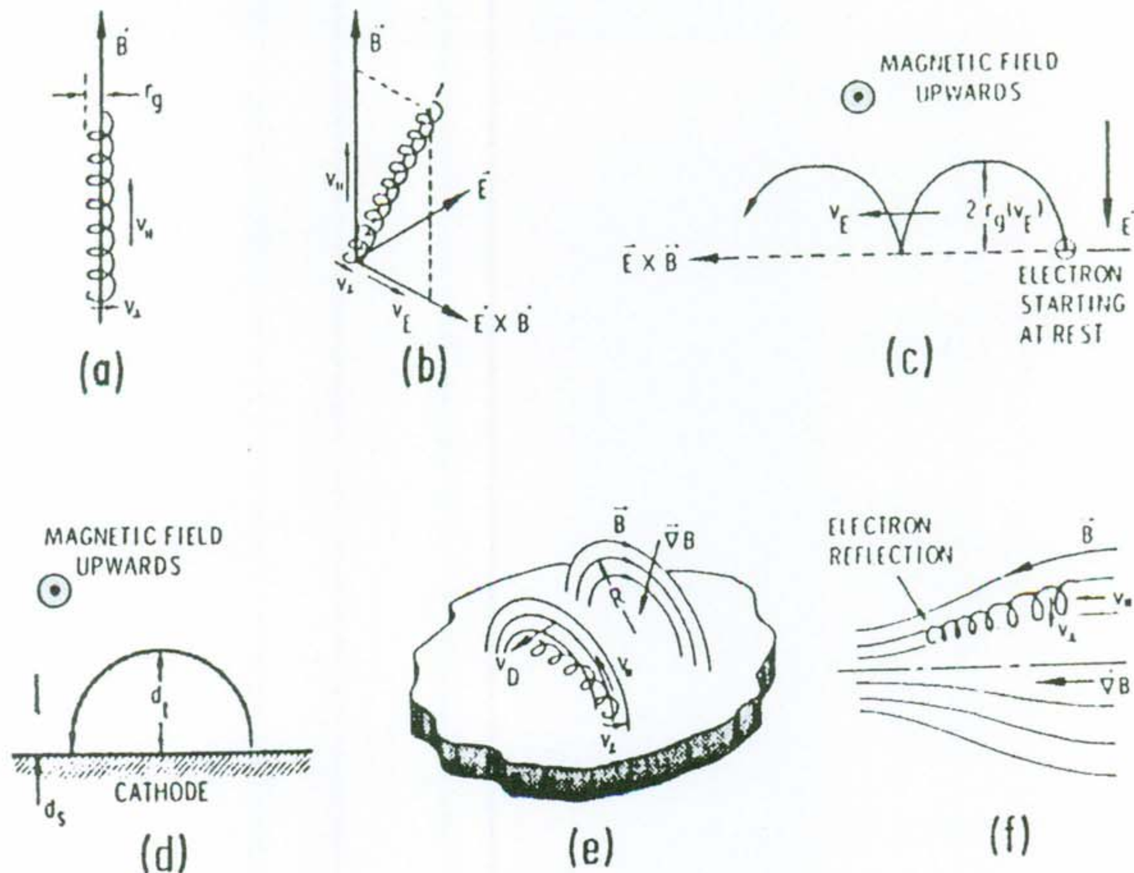

Fig. 3.3: ***Electron motion in static electric and magnetic fields***[21]

As a consequence, very high degrees of ionization are possible at relatively low pressure (in the range of 10^{-3}mbar). The magnetic field is shaped in a way to get plasma confinement. However, a general statement for magnetron construction is that magnetic field lines must "be born from the cathode and die onto the target". The high degree of ionization allows higher deposition rates at lower voltages in comparison to "normal" sputtering sources. This process is limited primarily by the ability to prevent the target from melting due to the high energy input from the ion bombardment.

3.5 Thin film physical structure

Thin film coatings are finding ever increasing applications in high technology solutions to material limiting problems. Due to the nonequilibrium nature of some vapor-deposition methods, the resulting film properties can be highly dependent on preparation parameters(22). In a number of cases it is the physical structure of the thin film which is either directly responsible for or related to the desired film property.

It is generally recognized that thin films prepared by physical vapor deposition show a wide range of microstructures and properties, both which are highly dependent on the preparation conditions. This has led to the development of the structure zone model (SZM)(23), which relates the microstructure of a thin film to the reduced temperature T/T_m (T_m = melting temperature) as a means of classifying the microstructures produced under different conditions.

It is usefully to envision coating process as a proceeding in three general steps:

- The first step involves the transport on the coating species to the substrate.
- The second step involves the adsorbtion of the substrate or growing coating, their diffusion over this surface, and finally their incorporation into the coating or their removing from the surface by evaporation or sputtering.

- The third step involves movement of the coating atoms to their final position within the coating.

The low temperature ($T/T_m<0.3$) zone 1 structure is columnar, consisting of tapered units defined by voided growth boundaries. The zone 2 structure ($0.3<T/T_m<0.5$) consists of columnar grains, which are defined by metallurgical grain boundaries and increased in width with T/T_m in accordance with activation energies typical of surface diffusion. The high temperature zone 3 ($T/T_m>0.5$) structure consists of equitaxed grains, which increase in size in accordance to activation energies typical of bulk diffusion.

According to this model, microstructural development is in turn controlled by shadowing effects (zone 1), surface diffusion (zone T and zone 2), and bulk diffusion (zone 3) as T/T_m increases.

The zone T structures are considered to be the internal structure of the zone 1

structures. The physical structure of a thin film is related to mobility of the adatoms at the growing film surface. For deposition processes removed

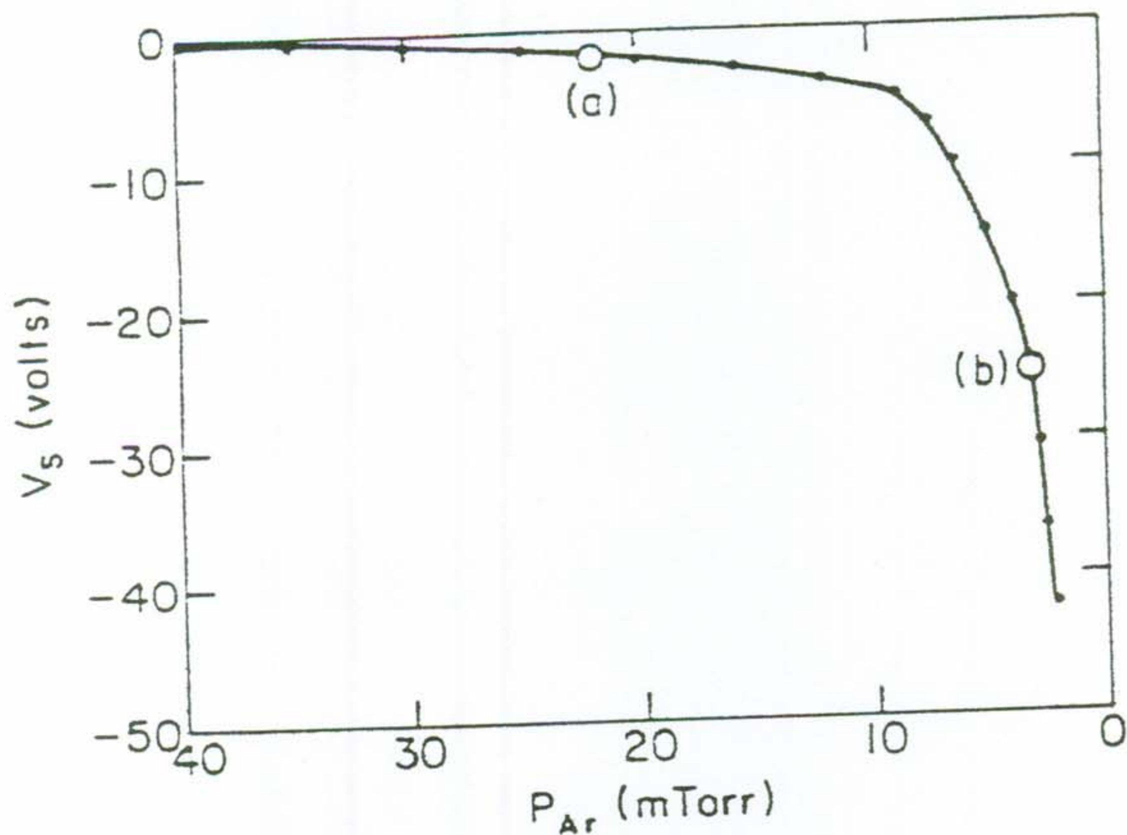

Fig. 3.4: ***Substrate bias potential (V_s) for a SiC target sputtered in Ar[22] effects of higher (a) and lower (b) pressure***

from equilibrium other sources of adatom energy are possible, and for sputtering, in particular, energetic particle bombardment can be an important process. The zone 1-T boundary is nonlinear and varies in a fashion similar to the film bias potential as a function of gas pressure (**fig. 3.4**). This V_s-induced mobility appears to be the more fundamental process affecting the physical structure and thus the SZM might be better represented by **fig. 3.5**. The zone 1-T boundary is drawn as a linear boundary since it is indicated that this is a reasonable approximation. Of course other effects besides V_s changes occur with decreasing sputtering gas pressure, such as an increase in the average energy of the sputtered species as they arrive at the growing film surface. This process, if dominant, would have a similar nonlinear energy dependence as in **fig. 3.4** and again would lead to a linear 1-T boundary. The **fig. 3.5**

representation of the SZM is still not perfect but it does clearly acknowledge the separate contribution of bombardment to adatom mobility and thus film physical structure.

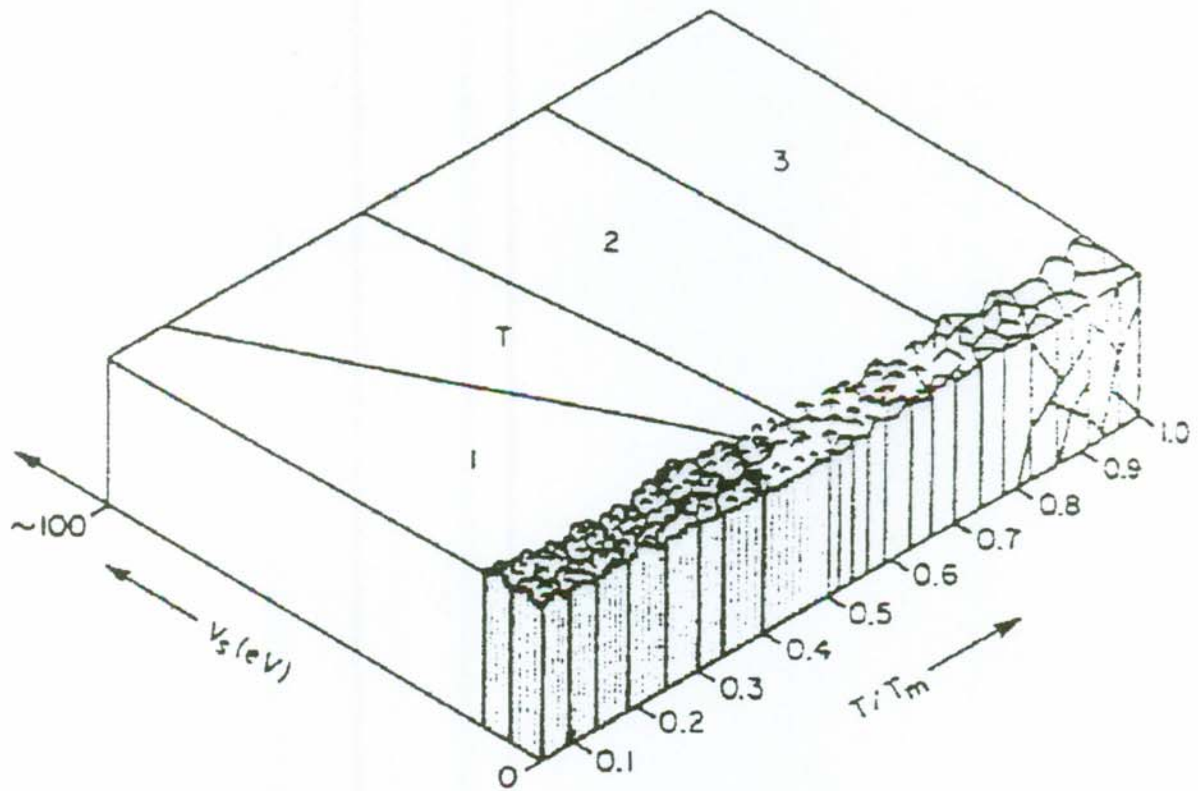

Fig. 3.5: ***effects of bombardment- and thermal induced mobility*** [22]

3.6 Current-voltage relation:

The current-voltage characteristic reveals a great deal about the ionization processes in a plasma discharge. The more efficient the discharge, the lower the voltage for a given current density (The current density in the erosion area of the target may be up to four times the average current densities given). Discharges operating in the magnetron mode obey an I-V-relationship of the form I proportional V^n, where n is an index to the performance of the electron trap and is typically in the range 5-9[24]. If the magnetic field is too weak, the discharge will leave the magnetron mode and the voltage will increase abruptly. This behavior is a result of electrons escaping from the trap without making sufficient ionization. At high magnetic field strength the discharge will extinguish. This is believed to be the result of electrons not achieving sufficient energy for ionization processes. At fixed voltage and magnetic field strength the current increases with pressure. For a given cathode configuration, a family of current-voltage curves versus pressure can be obtained that enable a suitable operating point to be chosen for a given power input.

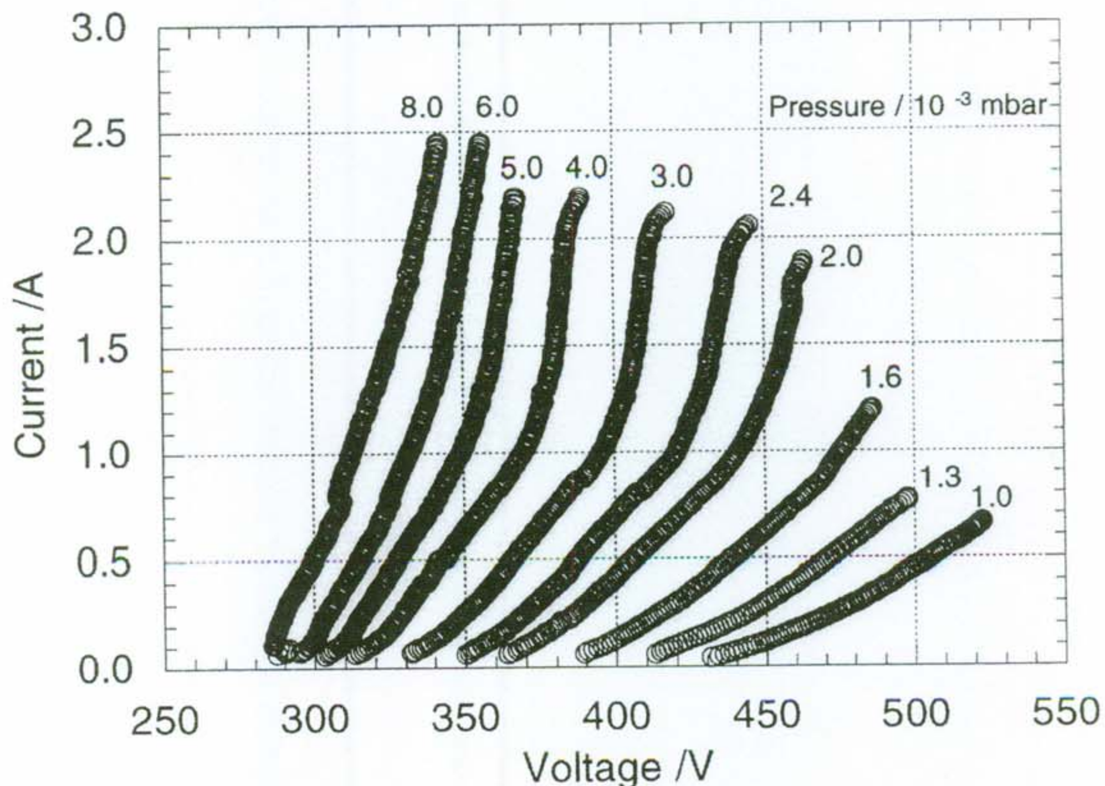

Fig. 3.6: ***current-voltage curves of the system used for the experiments to be mentioned***

3.7 Double magnetron

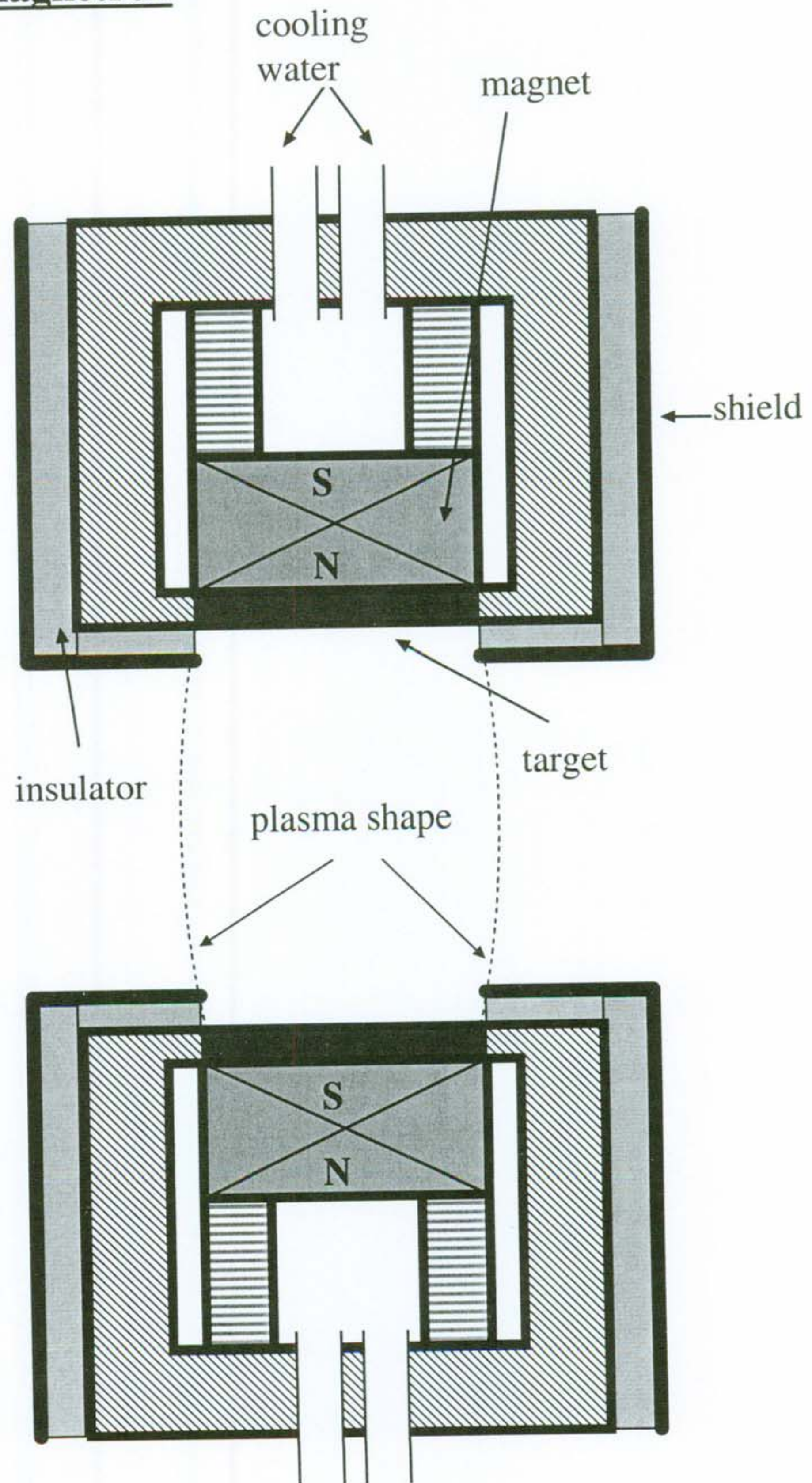

Fig. 3.7: ***The schematic diagram of the TFTS apparatus***

The non reactive sputtering of a compound as V_3Si requires two different targets of both materials. With respect to this requirement it can be convenient to use the target-facing-type sputtering (TFTS)(25). **Fig. 3.7** shows a planar magnetron system with facing two targets. Permanent columnar magnets are contained behind the target surfaces. The polarities of each internal magnet are opposite. In the application of usual planar magnetron sputtering, the ionizing electrons are confined by the magnetic field and the discharge plasma is produced in the toroidal region in front of the target surface. However, some of the trapped electrons escape from the region. When these escaping electrons are confined again, the discharge will be maintained at lower gas pressure than usual planar magnetron sputtering. This is done by facing two targets. Furthermore, it is also possible to improve utilization of the target material used for sputtering. The magnetic field distribution of usual planar magnetron sputtering generally results in the annular etching of the target shown in **fig. 3.8** In such a magnetron system, the target utilization is typically not more than 30%.

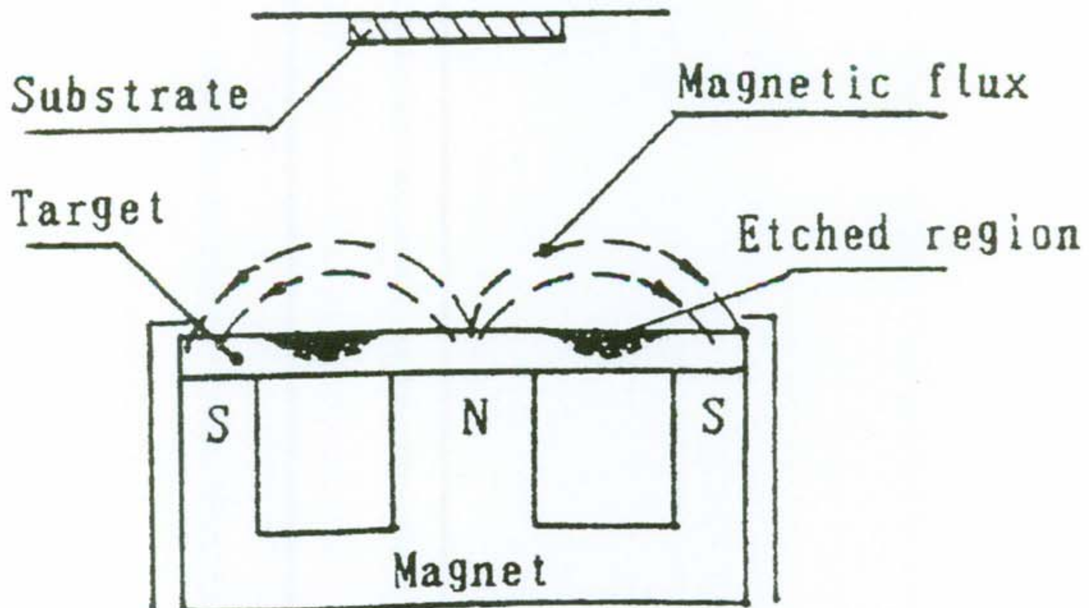

Fig. 3.8: ***The target configuration of planar magnetron sputtering method(25).***

Analysis of *Qihua Fan*[25] proved that the distribution of the magnetic field (i.e., the shape of the permanent magnet which engendered the magnetic field) has a close relationship with the uniformity of targets erosion. In the TFTS method a magnetic field perpendicular to the targets surface is used to confine the plasma. **Fig. 3.9** shows the differences in the distribution of perpendicular magnetic field strength at a distance of 10 and 30 mm away from the magnets surface. From **fig. 3.9 (a)** one could see the perpendicular component of magnetic field produced by the columnar magnet mainly concentrates in the vicinity of the common axis of the target. A great amount of plasma is confined in this region. This results in a high rate erosion of the target center area.
The perpendicular component of magnetic field engendered by the annular magnet relatively concentrates in the outer annular region shown in **fig. 3.9 (b)**. In this way the plasma not only can be confined in the region between the two facing targets and leads to high rate sputtering but also does not concentrate in some small region. This results in the improvement of uniformity of the target erosion and the target utilization increases to more than 50%.

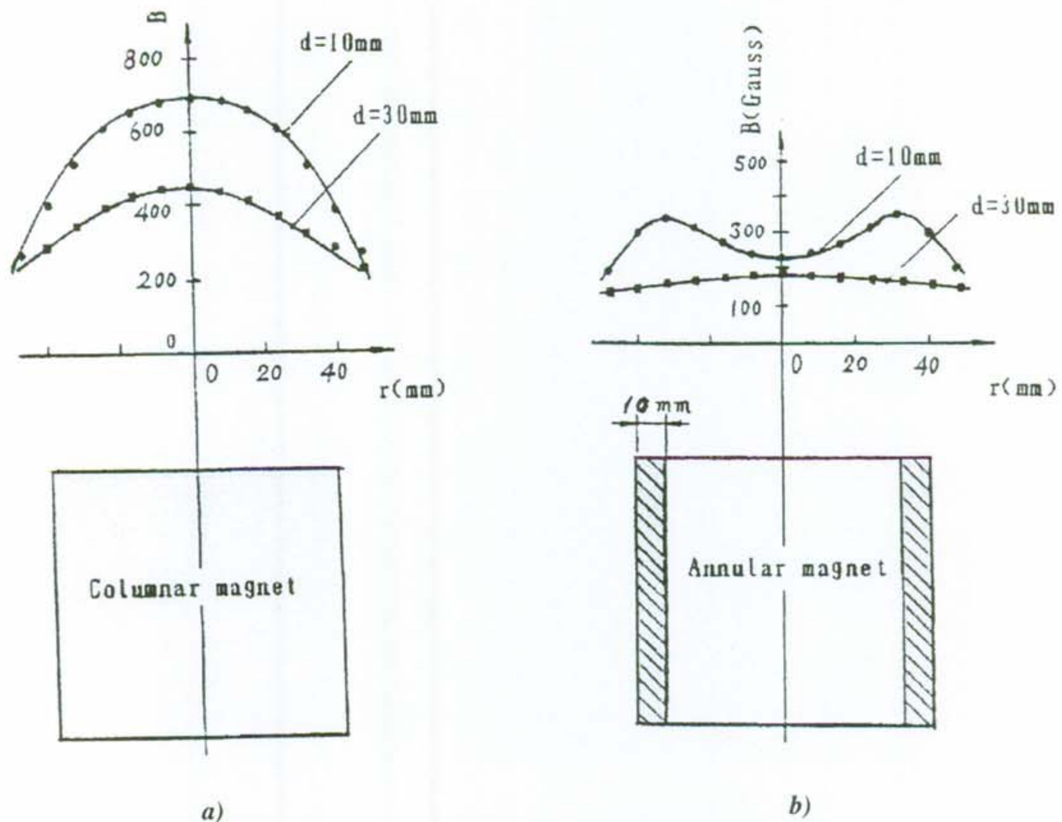

Fig. 3.9: The distribution of perpendicular component of magnetic field engendered by (a) columnar magnet, (b) annular magnet. d: vertical distance from the magnet surface. r: radial distance from the center of magnet surface

Fig. 3.10 compares the erosion profiles referring to the different magnets used inside the TFTS apparatus by *Qihua Fan*[25].

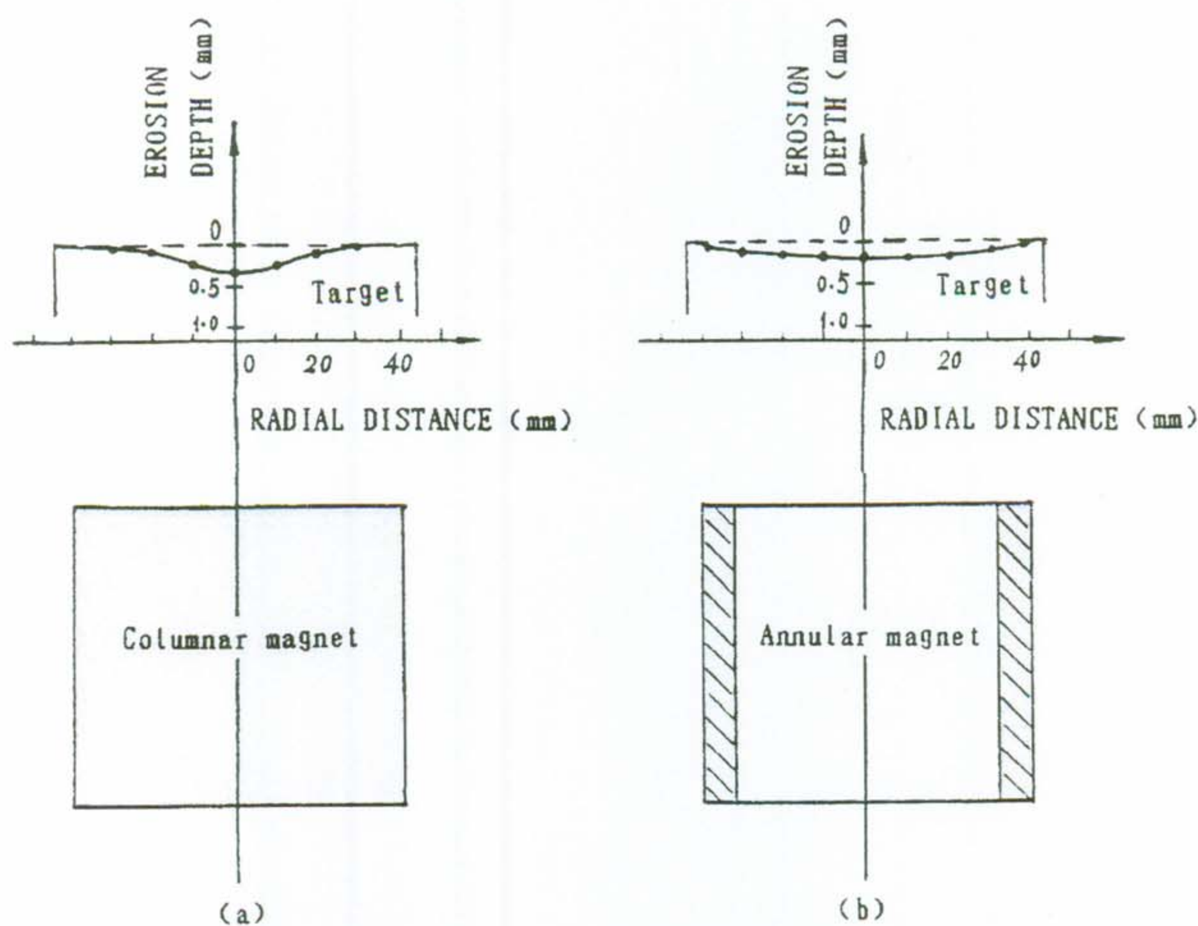

Fig. 3.10: ***Erosion profile of the target. (a) using columnar magnet, (b) using annular magnet.***

Another feature to be considered in target-facing-type sputtering is the uniformity of the deposited film. The film thickness distribution in the long side direction of a substrate is shown in **fig. 3.11** It is considered that the nonuniformity of the film thickness may be due to that the atoms and particles sputtered of from the targets have an approximate "cosine distribution"[25] in the profile planes perpendicular to the target surface. For sputtering with two targets consisting of the same type of material this distribution might not be a problem. For deposition of V_3Si two different targets are used to reach a deposition rate ratio equal to the stoichiometric ratio of 3:1.

Fig. 3.11 shows the film thickness distribution in the long side direction of a substrate between the two magnetrons.

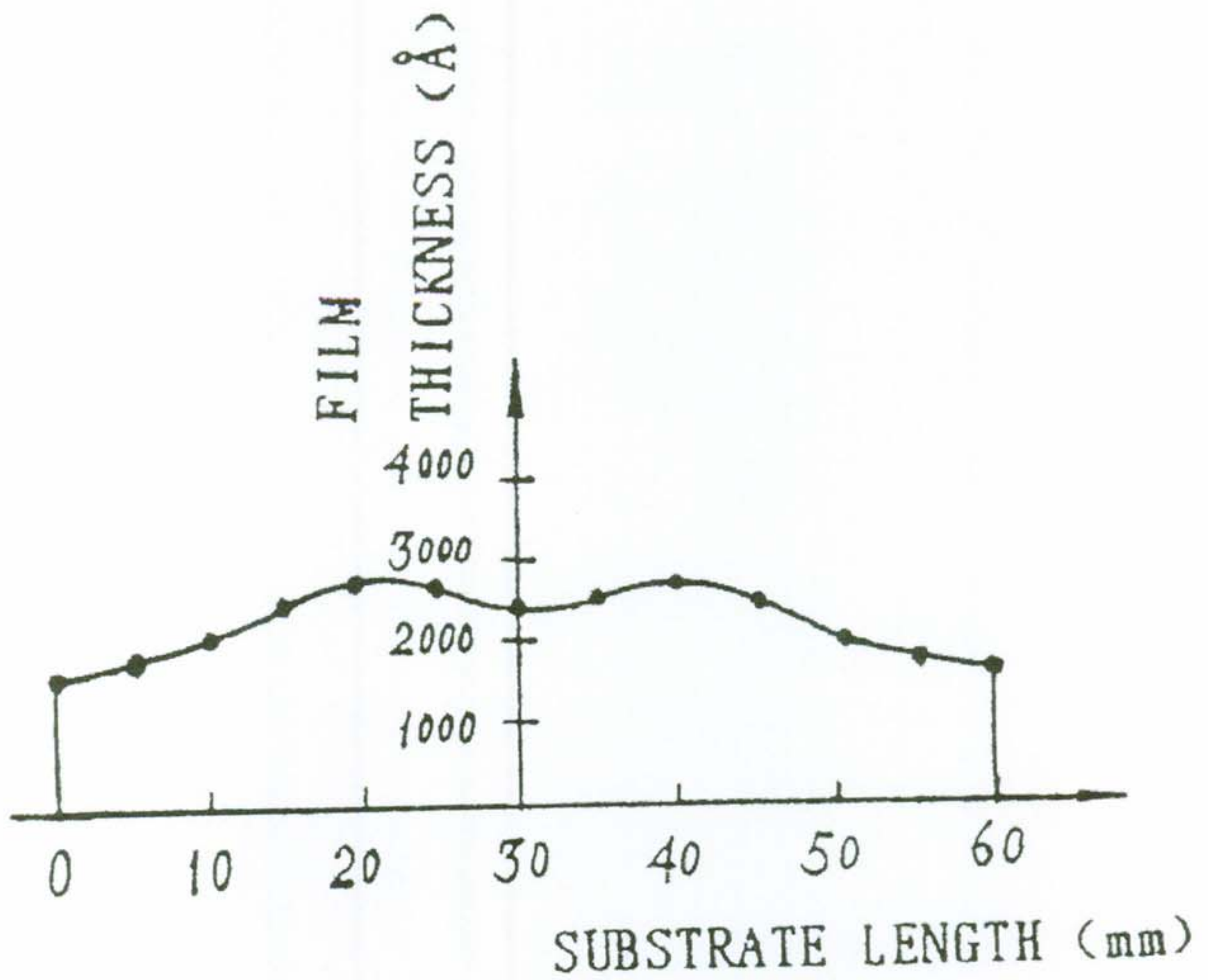

Fig. 3.11: ***Film thickness distribution in the long side direction of the substrate***

3.8 Residual resistivity ratio RRR

The superconductivity of V_3Si strongly depends on the right stoichiometric composition at a ratio of 3:1. In this case it is necessary to have a measurement device to get quick and accurate results of the composition. One feature of superconductors are effects of composition and atomic ordering on the electrical resistivity above the transition to superconducting state.

The residual resistivity ratio is defined as the ratio between the electrical resistivities at 300K and at 20K ($RRR=\rho_{300K} / \rho_{20K}$). Studies of *R.Flükiger et al*(11) on a series of single crystals show a sharp variation of the RRR quotient when approaching the stoichiometric composition.

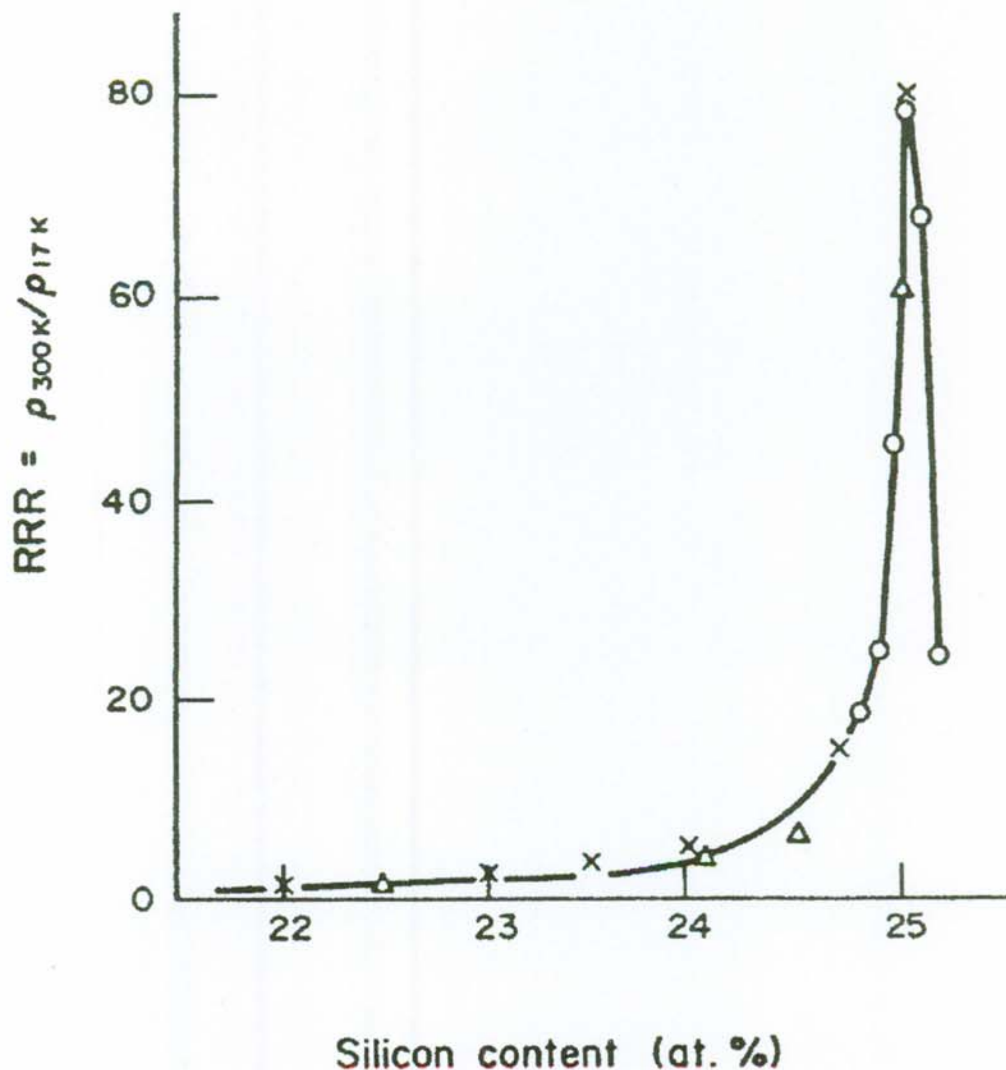

Fig. 3.12: ***Variation of the RRR value in V_3Si as a function of the silicon content***(11)

Between 22 at.% silicon and 24.5 at.% silicon, RRR increases from 1 to 6, while further addition of only 0.5 at.% silicon causes an increase up to RRR = 80! The nearly symmetrical behavior with respect to the stoichiometric composition indicates that the ρ_o is mainly dependent on the perturbation due to wrongly occupied sites, the identity of excess atom being of secondary importance. The behavior shown in **fig. 3.12** is certainly the most expressive way to demonstrate that this system is perfectly ordered; at the vicinity of the stochiometric composition, very small perturbations of the system (e.g. inhomogenities, small deviation from stoichiometry, small amounts of ternary additives or deviations from perfect ordering) may cause a considerable increase of ρ_o.

3.9 System requirements

Virtually any vacuum chamber can be used for magnetron sputtering, if it has been designed for a vacuum of 10^{-6} mbar or higher. The fact that the magnetron uses a magnetic field for plasma confinement, generally precludes the use of magnetic materials in the vicinity. Some viewing windows are strategically placed to monitor the progress of the sputtering process and anomalies of the discharge. Furthermore the system contains some feedthroughs. These are namely for:

- passage of electrical signals from monitors: pressure, thickness, temperature etc.
- power supply and cooling water of the magnetrons
- supply of movement for the sample holder and the exchange of the samples

The pumping system must be capable of pumping the chamber to a vacuum of 10^{-7} mbar in a reasonable time and maintain a pressure between 10^{-3} and 10^{-2} mbar while gas is being supplied to the system. As in many common systems we make use of a rotary pump followed by a turbo-molecular pump(26).

The simplest method to control the gas supply consist of a leak valve directly fed by the gas cylinder. It is necessary to reduce the pumping speed in order to achieve the necessary supply of gas.

It has been shown that the current-voltage characteristic of a magnetron discharge follows a quadratic law. The maximum current that any magnetron can stand depends mostly on the efficiency of the cooling system. One rough estimate can be made by allowing for a maximum current density of 0.25 A/cm^2 on the region of the target where erosion is higher. Having estimated the maximum allowable current, it is easy to choose a power supply. The power supply must have a current rating equal to the maximum current and voltage rating in excess of 600V. It is important that it can be controlled in constant current mode because the discharge can be unstable and because it is the current that relates directly to the rates of erosion and deposition.

3.9.1 Sketch of the system

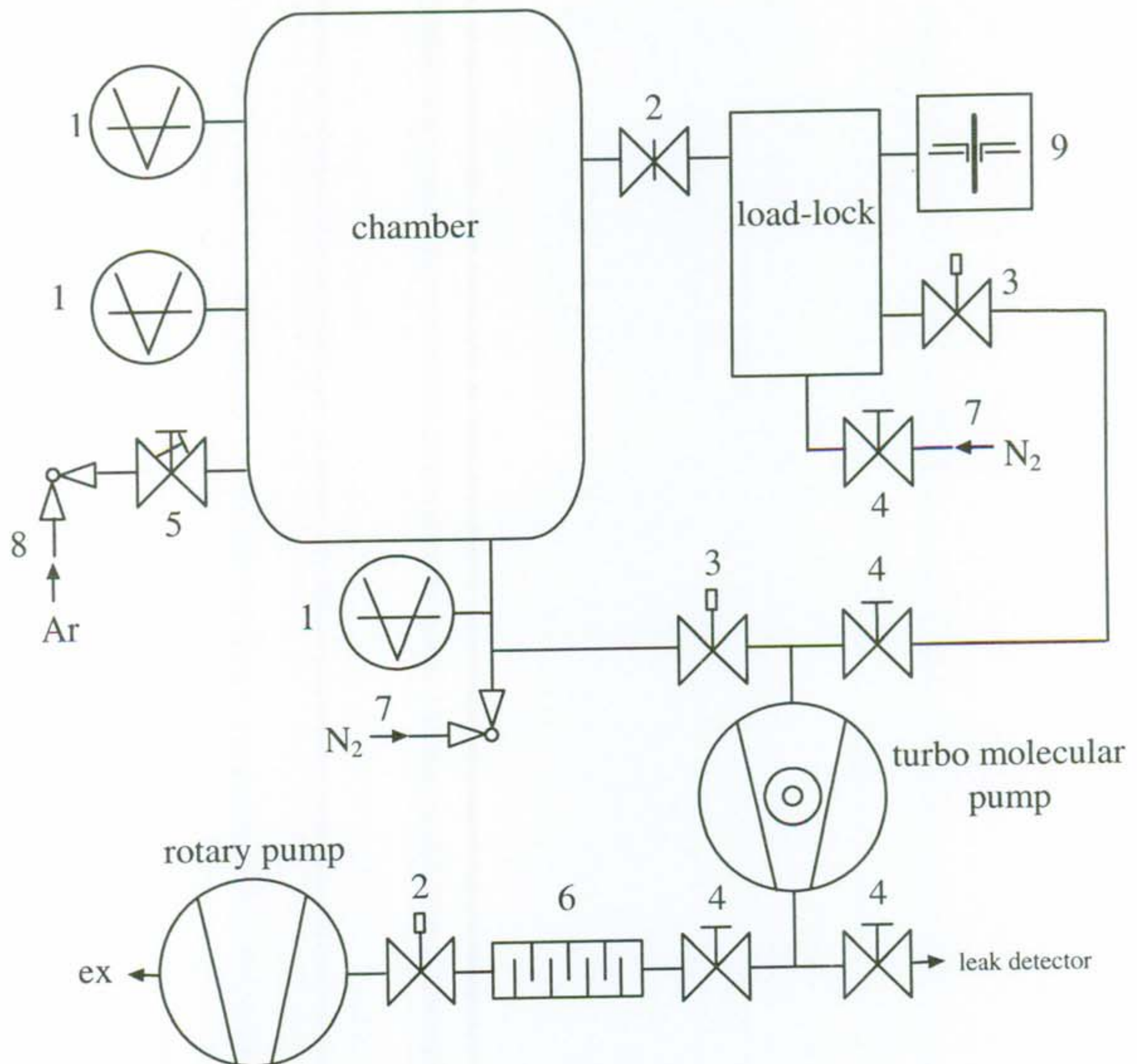

Components:

Rotary pump :	Leybold-Heraus Trivac	1	pressure gauges
Typ :	D 25 BCS	2	gate valve
pumping speed :	$S = 25\ m^3/h$	3	electromagnetic valve
ultimate pressure :	8×10^{-4} mbar	4	manual valve
Turbo pump :	Pfeiffer Balzers	5	variable-leak valve
Typ :	TPU 330	6	trap
(bakeable)		7	N_2-inlet valve
pumping speed :	$S = 300\ l/s$	8	Ar-inlet valve
ultimate pressure :	5×10^{-8} mbar	9	linear motion leadthrough(*)

(*) The linear motion leadthrough in combination with the gate-valve made it possible to position and to change the sample holders without opening the chamber.

3.10 Measurement Techniques

Film thickness measurements

The thickness is measured with the stylus method. The principle of this method is as follows: A diamond needle with a tip radius of about 10 μm serves as electromechanical pick-up. The vertical movement of the needle, when it slides over the film substrate step, can be measured and directly read-out on a monitor. The measurement range spans from 200Å to a few μm. Presupposition for the application of this method is a sufficient hardness of the film and a plan surface.

Residual resistivity ratio measurements

The RRR of the V_3Si coatings on insulating quartz substrates is measured with the four point method in order to eliminate the effect of possible contact resistance at the contact points between the film and the pins of the measuring device. After measurement of the film resistance at room temperature the samples are cooled down in a helium bath to 8 °K. This value of temperature is far below the transition temperature of V_3Si ($T_c \approx 17K$), but due to deviation in composition a transition to superconducting state could occur at temperatures down to 10K[27].

4. Sputtering Experiments

4.1 Configuration of the sputtering system

The magnetron configuration as shown in **fig. 3.7** is mounted in a columnar vacuum chamber pumped by a rotary pump and an turbo molecular pump. We achieved an ultimate pressure of 3×10^{-7} mbar after 24 hours of pumping. After sputter cleaning the pressure reduced to 3×10^{-8} mbar. Due to the fact that there are no literature results about Target-Facing-Type-System Cosputtering with two different targets, we did the characterization sputtering for the U-V relations with niobium targets, also in order to sort out a suitable distance for the magnetron. A distance of 47-50 mm came out to fit best. There were usually mounted two samples on a substrate holder.

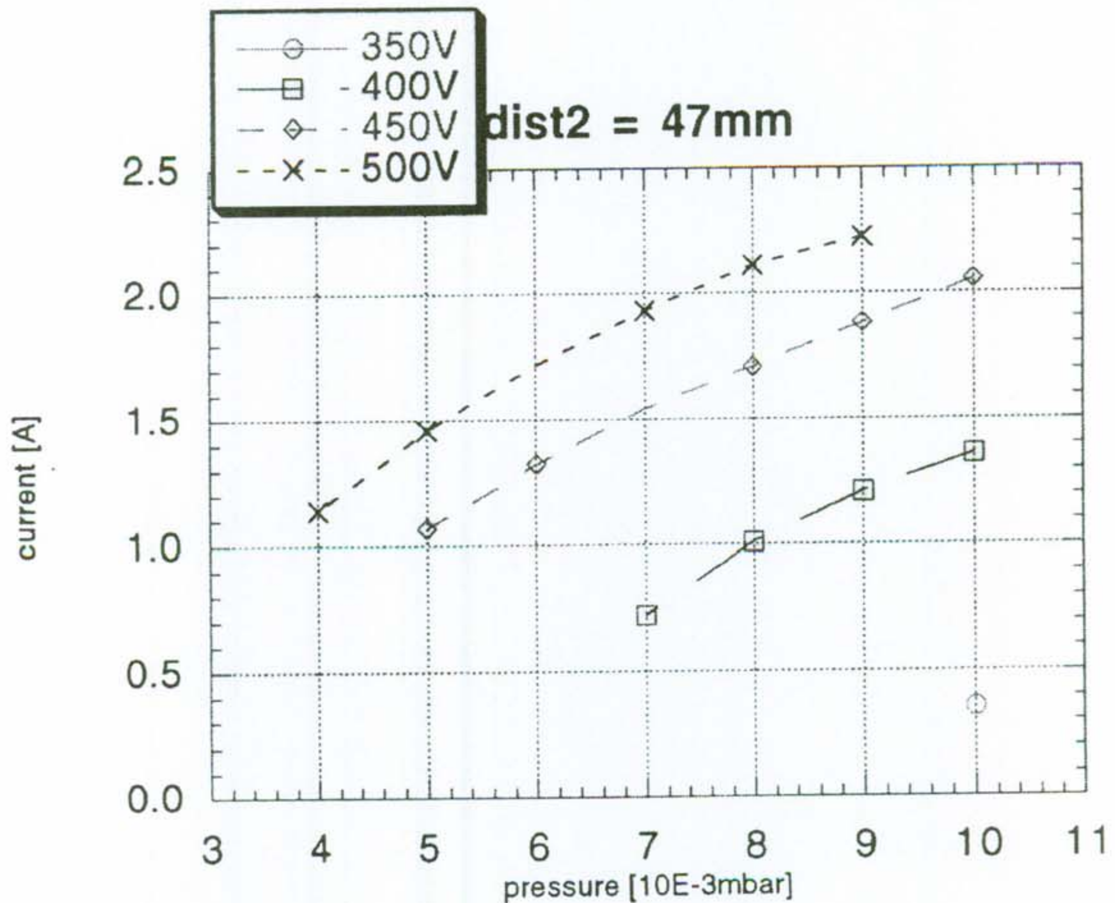

Fig. 4.1: *chosen magnetron distance*

4.2 First V_3Si - Sputtering

The primary goal for the first sputtering attempts was to prepare films with a good stoichiometry, so that we could expect superconductivity. Regarding the influence of horizontal distance between substrate and target (**fig. 3.11**) and the different strength of the desired particle beams from the targets suggested a I_V/I_{Si} ratio below 3/1. Despite using various ratios there occurred no superconductivity. The **EBS** analysis (electron beam scattering) of some of the samples showed different composition depending on different electron beam energies. This could be traced back to accumulations in the substrate or background signals of the quartz (SiO_2) samples.

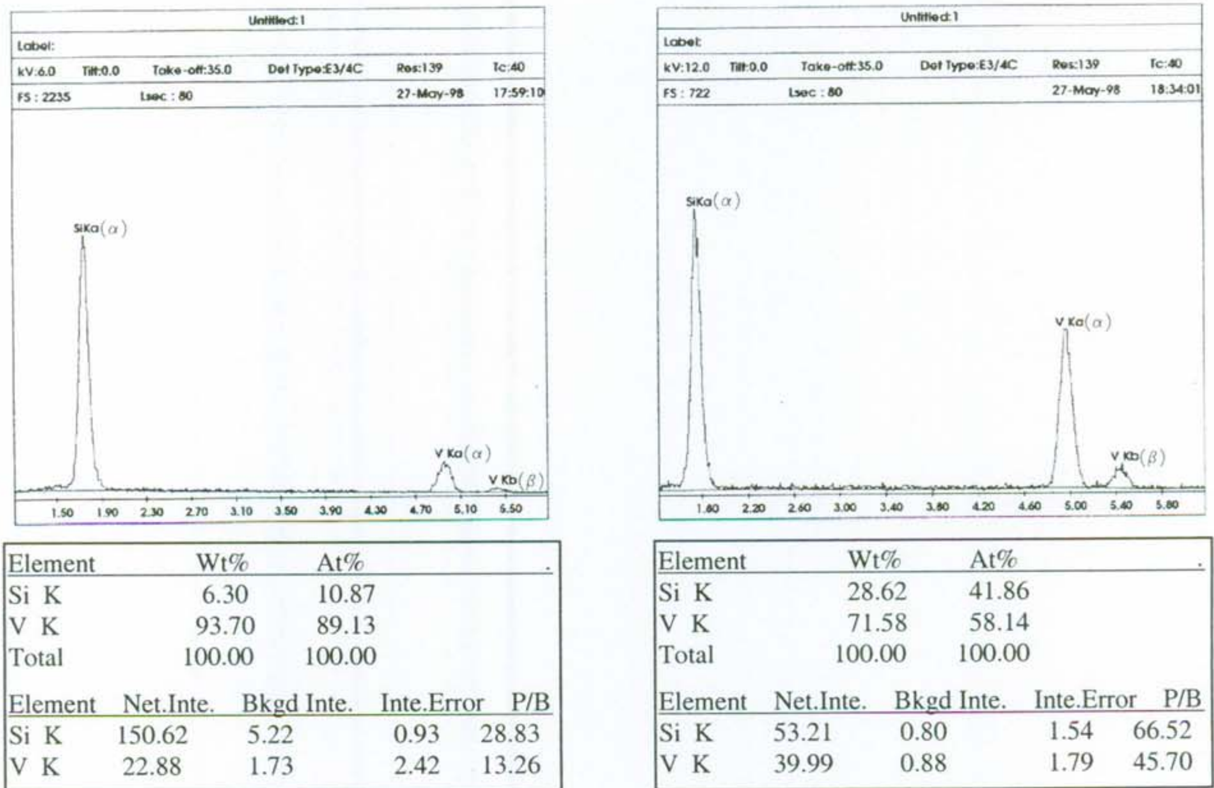

Element	Wt%	At%
Si K	6.30	10.87
V K	93.70	89.13
Total	100.00	100.00

Element	Net.Inte.	Bkgd Inte.	Inte.Error	P/B
Si K	150.62	5.22	0.93	28.83
V K	22.88	1.73	2.42	13.26

Element	Wt%	At%
Si K	28.62	41.86
V K	71.58	58.14
Total	100.00	100.00

Element	Net.Inte.	Bkgd Inte.	Inte.Error	P/B
Si K	53.21	0.80	1.54	66.52
V K	39.99	0.88	1.79	45.70

Fig. 4.2: ***EBS analyse of Sample #14 at 6 keV and 12 keVelectron beam enrgy***

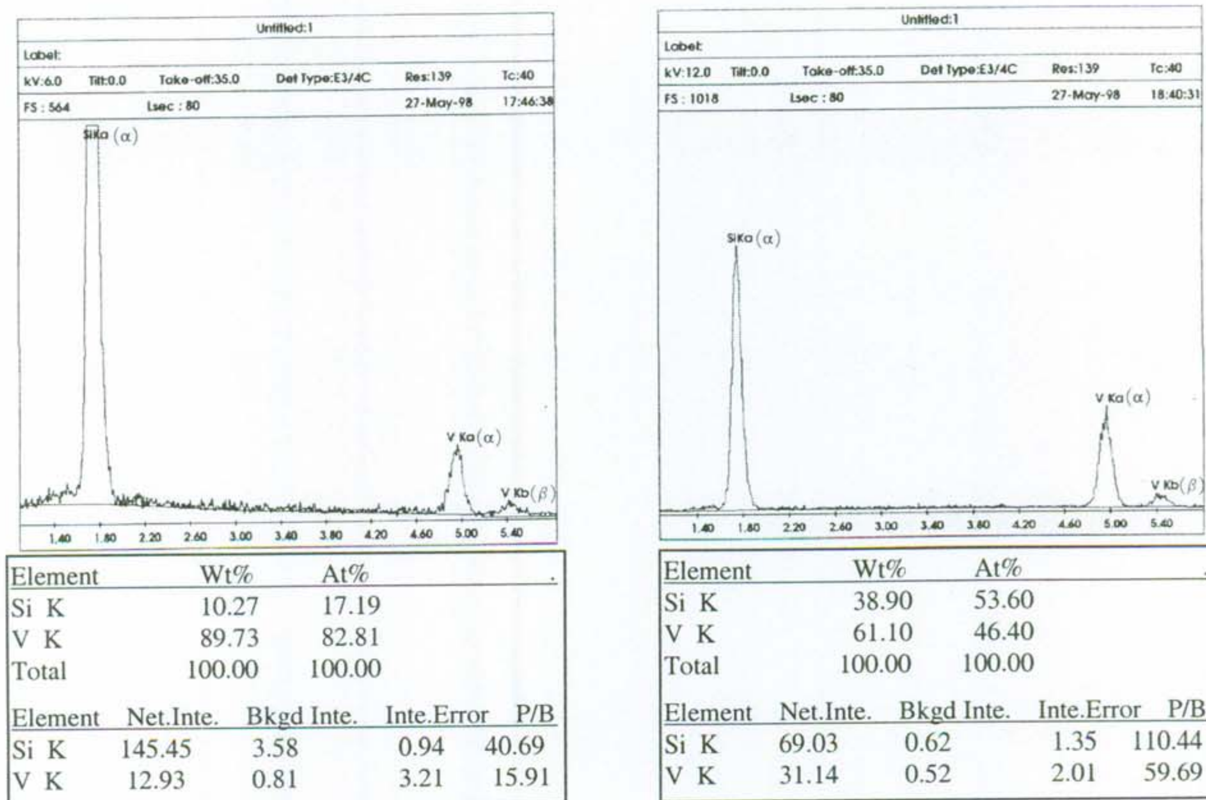

Element	Wt%	At%
Si K	10.27	17.19
V K	89.73	82.81
Total	100.00	100.00

Element	Net.Inte.	Bkgd Inte.	Inte.Error	P/B
Si K	145.45	3.58	0.94	40.69
V K	12.93	0.81	3.21	15.91

Element	Wt%	At%
Si K	38.90	53.60
V K	61.10	46.40
Total	100.00	100.00

Element	Net.Inte.	Bkgd Inte.	Inte.Error	P/B
Si K	69.03	0.62	1.35	110.44
V K	31.14	0.52	2.01	59.69

Fig. 4.3: ***EBS analyse of Sample #16 at 6 keV and 12 keV electron beam energy***

Nevertheless the relation of the voltages slightly below 2 (U_V/U_{si}) corresponded to the best so far achieved RRR values. Within the range of the used voltages there must have formed films with composition where superconductivity in respect of stoichiometry could have been expected. The failure based on drastically disorder in the structure of the films. According to the revised structure zone model for thin films by *Messier*, *Giri* and *Roy*[22] the structural disorder is caused by less adatom mobility of the striking atoms. A heater mounted in the vicinity of the substrate holder appeared to be an easy way to give an extra contribution of energy to the depositing atoms.

All the samples, which were sputtered in this manner, showed superconductivity.

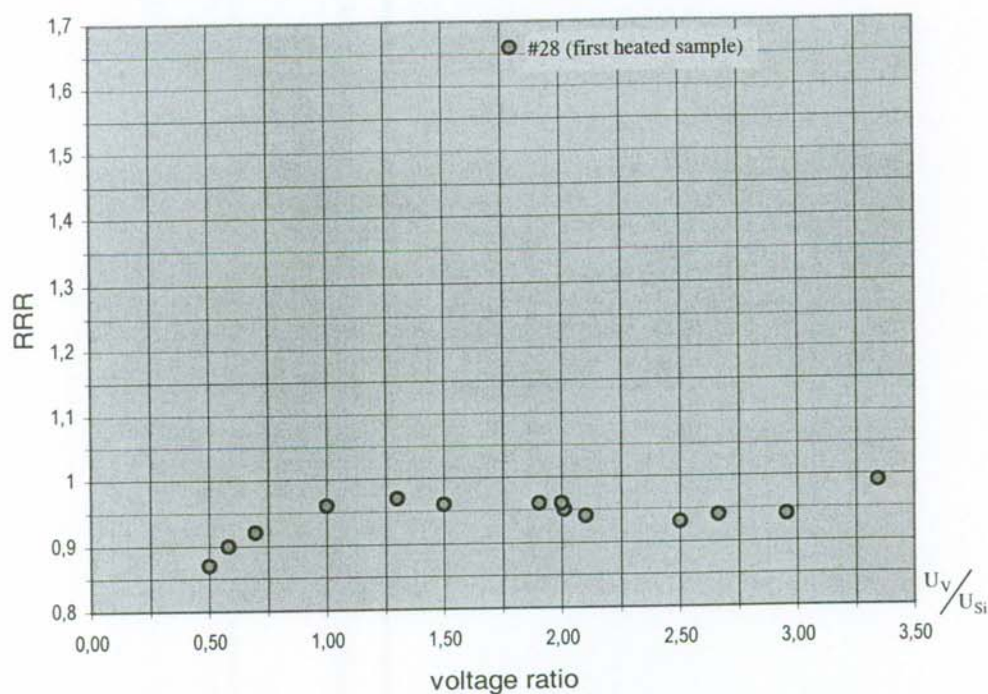

Fig. 4.4: ***First sputtering series with one heated substrate***

To determine the stoichiometrically composition, two samples were analyzed by **RBS** (**R**utherford **b**ack**s**cattering)[(28)]. The ion beam used in the RBS measurements was a 1.8 MeV alpha (He4) beam and the detector was put at 30 degree to the beam line. In spite of weakly RRR and T_c properties the spectrum was in accordance with a simulation of V_3Si.

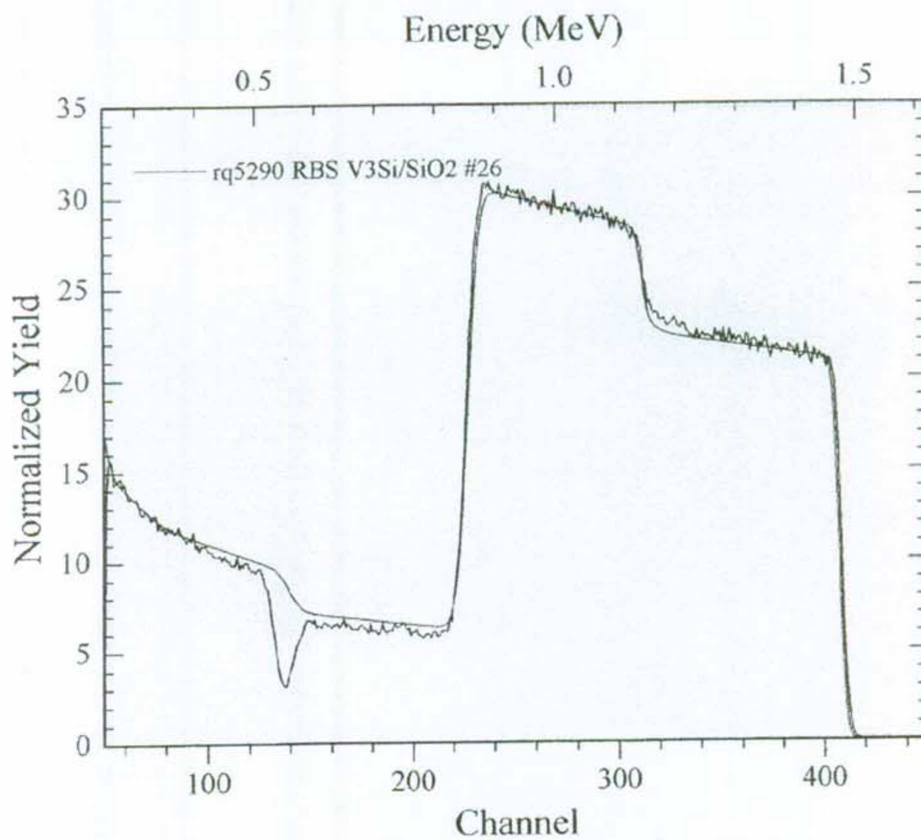

Fig. 4.5: ***RBS analyse of sample #26***

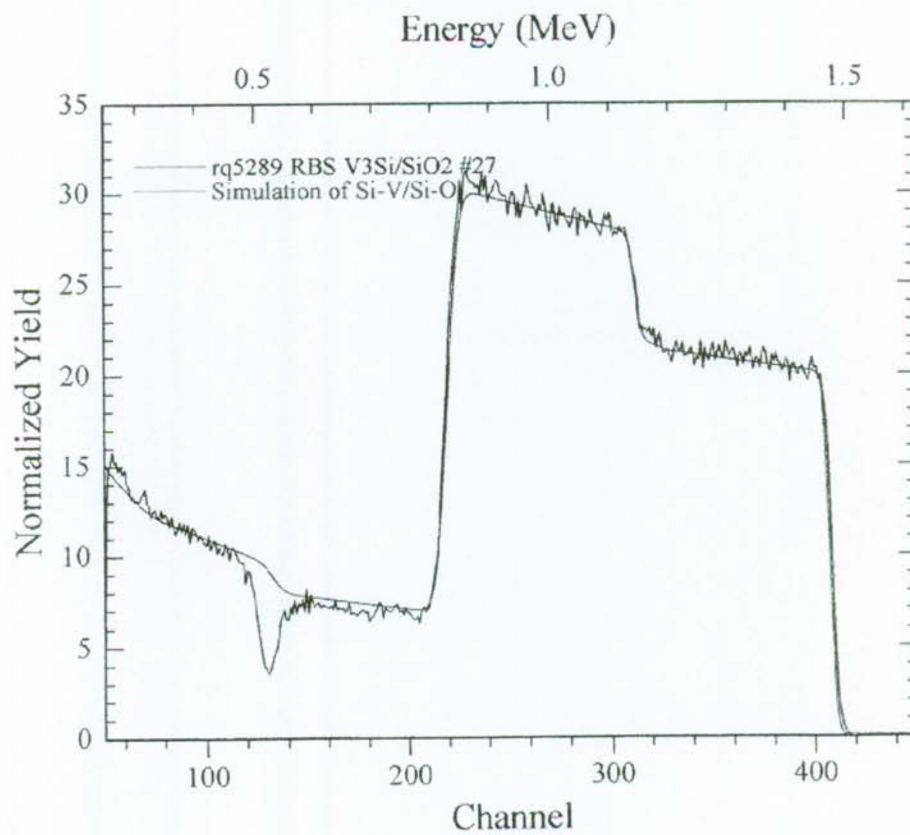

Fig. 4.6: ***RBS analyse of sample #27***

4.3 Sputtering with a Substrate Heater

The following samples were prepared at temperatures of 500 °C and varying U_V/U_{si} values. The effects of the different U_V/U_{si} were limited to an ultimate RRR of 1.77 and T_c's up to 11.5 °K, but the graphics 4.7, 4.8 have shown an obvious tendency for a suitable voltage ratio surrounding 2.35-2.40.

RRR versus voltage ratio

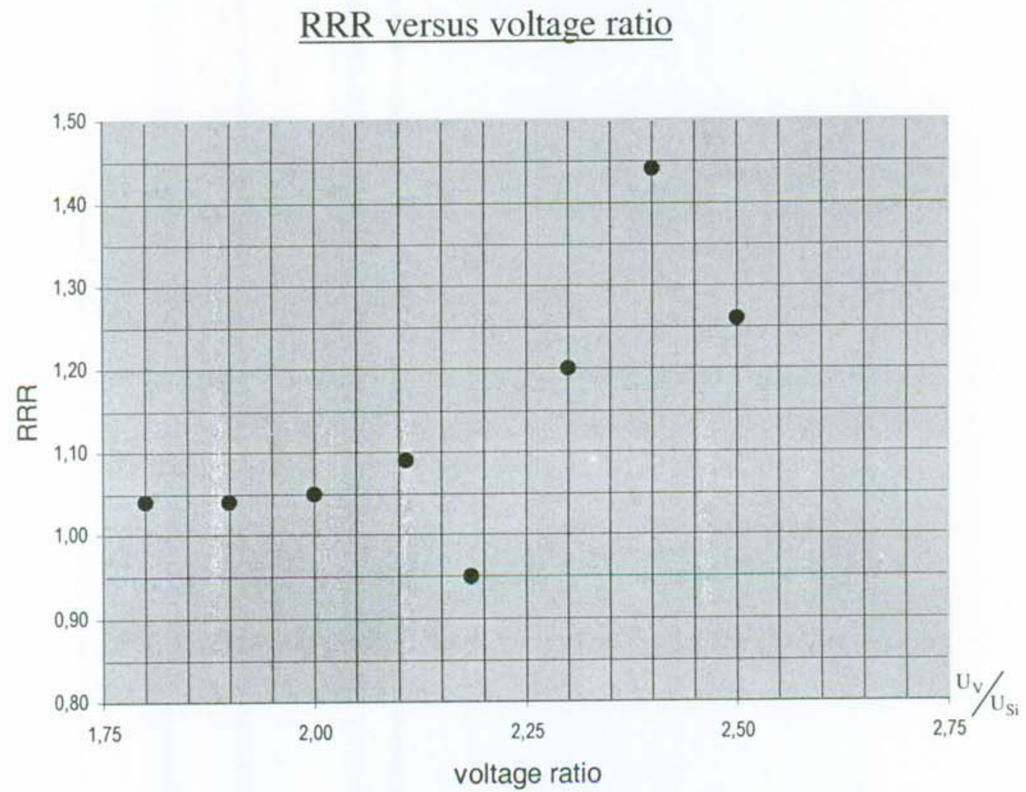

Fig. 4.7: ***Sputtering with heater 26/06/98***

RRR versus voltage ratio

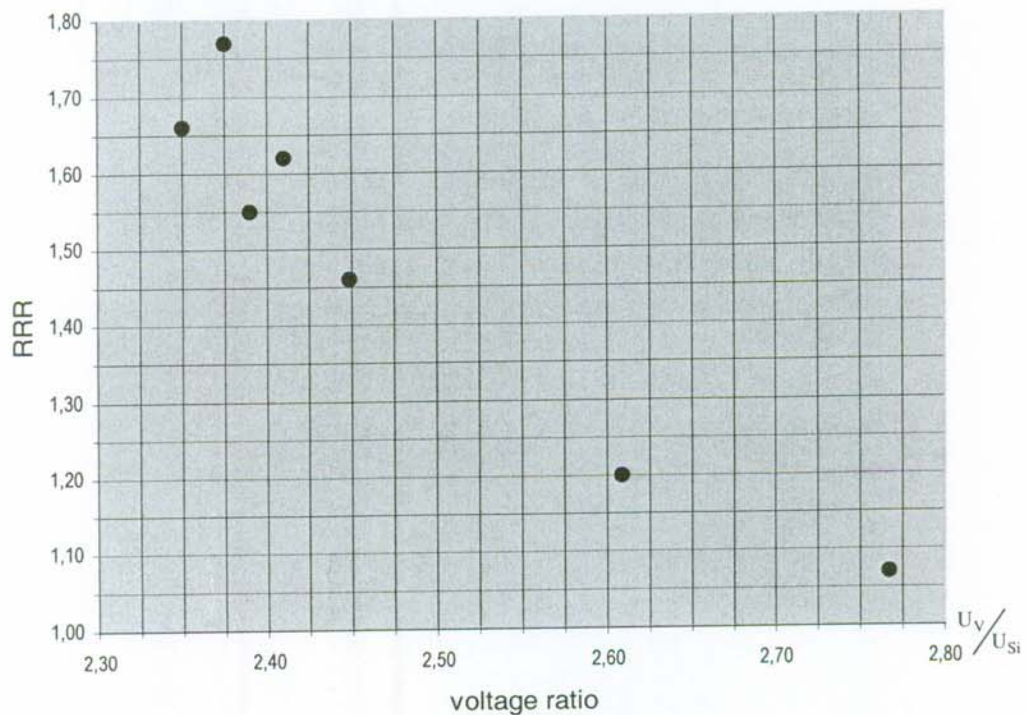

Fig. 4.8: ***Sputtering with heater 03/07/98***

Due to limitations of the deposition system, we could not sputter at temperatures higher than 500 °C. As shown by *Moore, et al.*[(30)], at Stanford in their tunneling studies, the best quality V_3Si thin films (highest T_c's and resistance ratios RR) are obtained for „hot„ and „slow„ depositions, specifically depositions at substrate temperature $T \cong 850$ °C and at deposition rate ≤ 3 nm/sec. Higher resistivity films (with correspondingly reduced T_c's) were obtained by depositing at lower substrate temperatures[(30)].

The final samples, which were annealed at 800 °C after sputtering reached RRR of 12.3 and T_c of 15.9 °K.

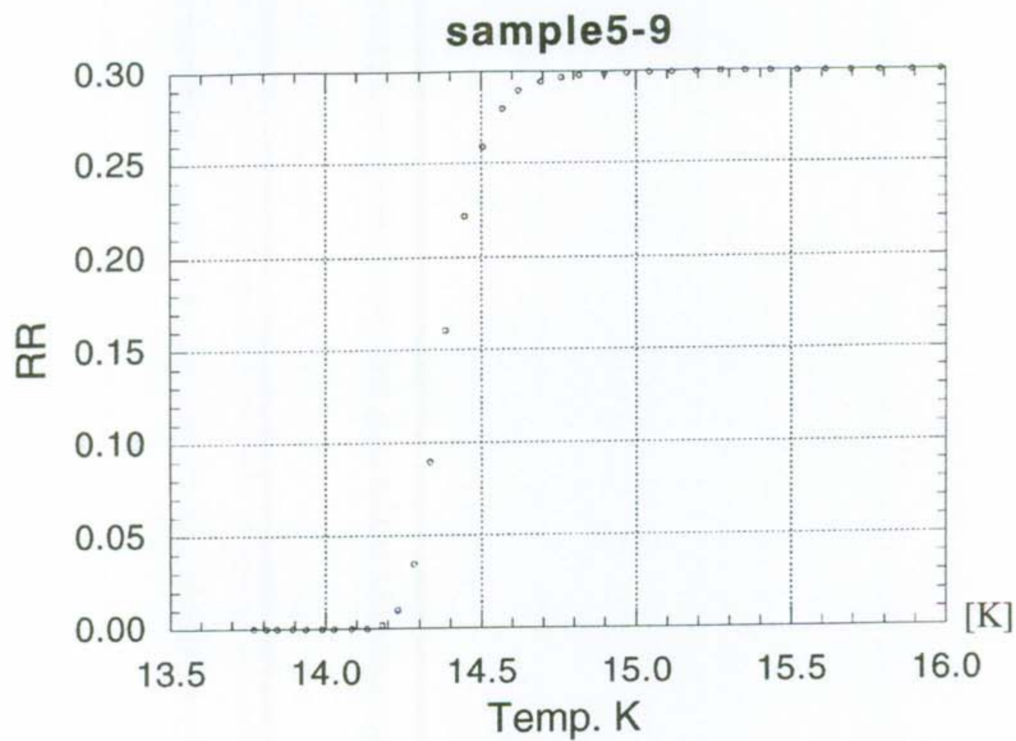

Fig. 4.9: *sputtered at 500 °C, annealed at 800 °C, thickness 0.6 µm, RRR 3.3*

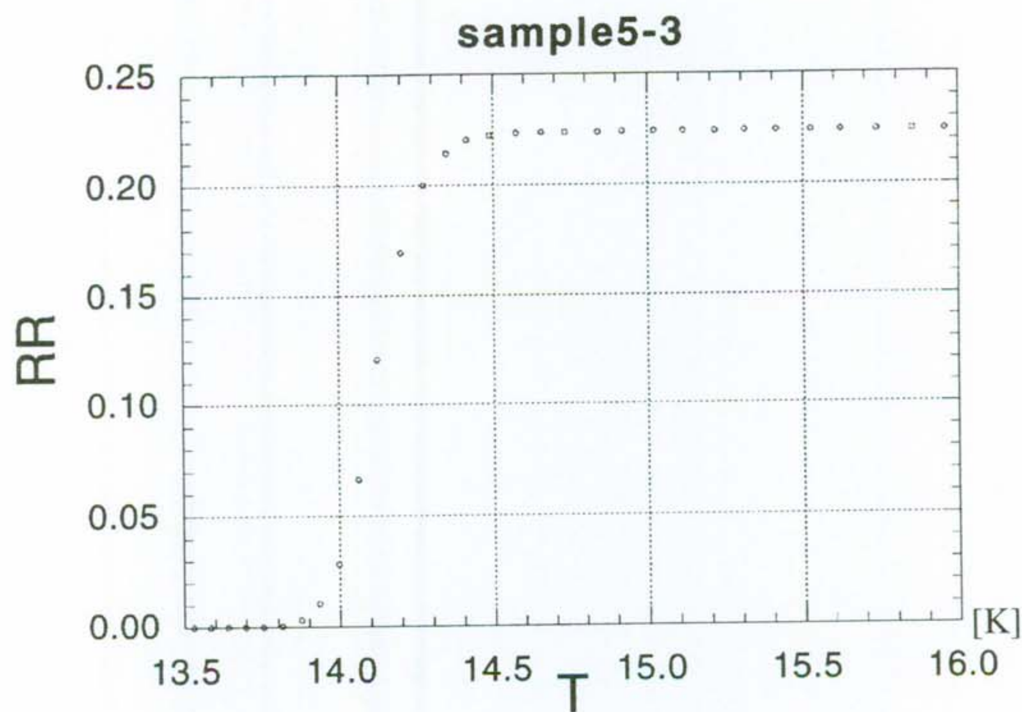

Fig. 4.10: *sputtered at 500 °C, annealed at 800 °C, thickness 0.6 µm, RRR 4.3*

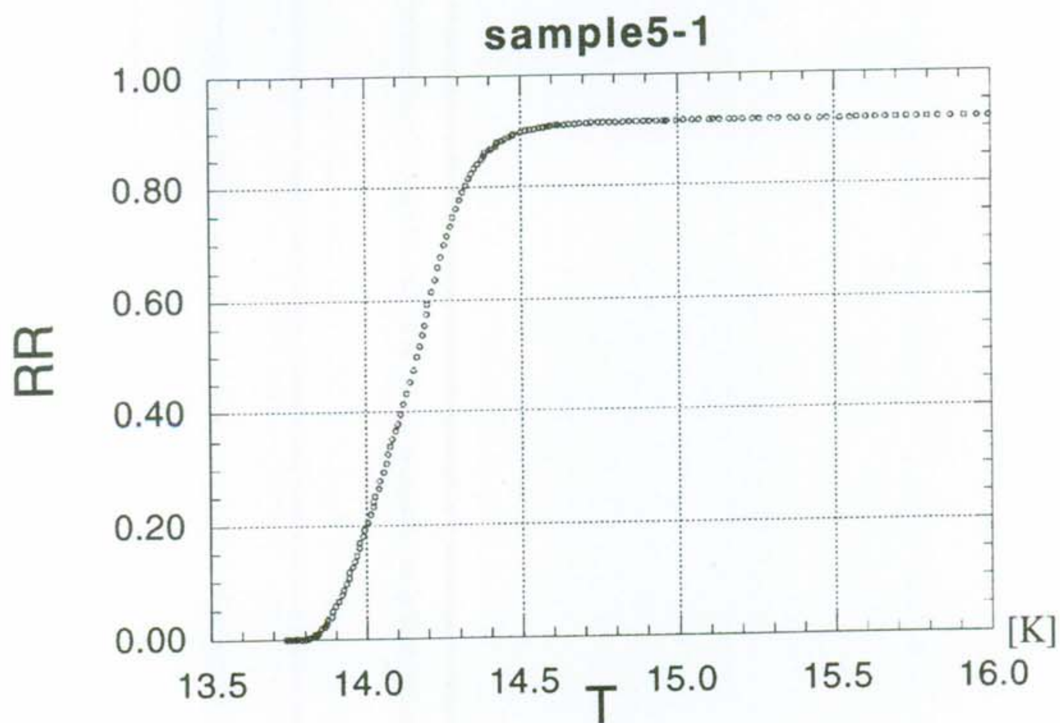

Fig. 4.11: *sputtered at room temp., annealed at 800 °C, thickness 0.6 µm, RRR 4.5*

4.4. V_3Si Cosputtering without heating

Sample	P_{Ar} [mbar]	I_V [mA]	I_{Si} [mA]	U_V [V]	U_{Si} [V]	U_V/U_{Si}	Time [min]	R300 [mΩ]	RRR
4	5.0 E-2	300	100	1152	555.5	2,07	25	5425.9	0.92
6	5.0 E-2	300	150	985	490	2,01	4 x 5	4466	0,95
7	5.0 E-2	450	250	979	331,5	2,95	10,85	2005,5	0,94
9	5.0 E-2	600	400	962	361	2,66	2 x 5,5	2476,6	0,94
11	5.0 E-2	405	180	1062	317,5	3,34	2 x 10	4344	0,99
13	5.0 E-2	420	390	518	518	1,00	2 x 10	4309	0,96
15	5.0 E-2	360	400	424	607,5	0,70	20	3135	0,92
17	5.0 E-2	350	428	402	692	0,58	15	2926	0,9
18	5.0 E-2	315	424	393	787,5	0,50	10	6652	0,87
19	2.0 E-2	360	220	814	418,5	1,95	-	-	
20	8.0 E-3	301	140	1015	533	1,90	13	1631	0,96
21	2.0 E-2	286	155	840	420	2,00	15	1709	0,96
22	5.0 E-2	475	330	735	350	2,10	10	8650	0,94
23	5.0 E-2	475	305	860	344	2,50	11	6642	0,93
24	2.0 E-2	381	200	1000	400	2,50	10	-	
26	2.0 E-2	312	225	653	435	1,50	10	1431	0,96
27	2.0 E-2	329	270	621	477,5	1,30	11	1357	0,97
28*	2.0 E-2	404	380	917	511	1,79	7,5	1951	1,66

* heated during sputtering
begin: 312°C
end : 274°C
Tc ~ 9 - 10 °K

4.5. V_3Si Cosputtering with heated substrate I

Date 26/06/98 | No. 1

Heater 40 V | Temp. 500°C | Po 5.4 E 07 | Bake 8h

Rv 2.5 MΩ | Rsi 0.8 MΩ | Rvsi 4.5 MΩ | XTC 81%

Sample	1	2	3	4	5	6	7	8
P_{AR} mbar	2 E-02	2 E-02	2.4 E-02	2.7 E-02	3.0 E-02	3.5 E-02	5.0 E-02	2.0 E-02
I_V A	0.31	0.33	0.36	0.38	0.38	0.39	0.37	0.34
I_{si} A	0.19	0.21	0.22	0.22	0.22	0.22	0.22	0.22
U_V V	925	942	976	970	973	960	920	900
U_{si} V	487	471	463	444	423	400	368	500
U_V/U_{si}	1,90	2,00	2,11	2,18	2,30	2,40	2,50	1,80
T °C	503	500	500	502	500	501	503	499
Time min	15	15	15	14	15	15	15	15
Rate Å/s	-	3.3	3.3	3.5	3.3	3.3	1.7	-
Thick. 10kÅ	-	0.3	0.3	0.3	0.3	0.3	0.15	-
R_{300} mΩ	9737	3937	3420	4444	3035	2619	4540	8947
RRR	1,04	1,05	1,09	0,95	1,20	1,44	1,26	1,04
Tc K	-	-	< 9.0	< 9.0	< 9.25	< 10.6	< 9.5	-
ΔTc	-	-	> 1.0	> 0.8	> 0.5	> 0.4	> 0.4	-

4.6. V_3Si Cosputtering with heated substrate II

Datum No. 2
03/07/98

Heater 40V Temp. 500 °C Po: 4.5 E -07 Bake 2h XTC 83%

Sample	1	2	3	4	5	6	7	8
P_{AR} mbar	7.5 E-02	7.0 E-02	5.0 E-02	4.0 E-02		4.0 E-02	4.0 E-02	4.4 E-02
I_V A	0.30	0.37	0.38	0.34		0.34	0.35	0.33
I_{Si} A	0.13	0.20	0.22	0.22		0.19	0.19	0.17
U_V V	985	960	950	940		956	964	950
U_{Si} V	356	368	388	400		400	400	400
U_V/U_{Si}	2,77	2,61	2,45	2,35		2,39	2,41	2,38
T °C	498	500	505	504		504	503	600
Time min	25	30	30	30		30	30	30
Rate Å/s	1.0	1.2	1.8	2.1		2.0	2.1	1.6
Thick. 10kÅ	1.5	2.1	3.3	3.9		3.7	3.9	2.9
R_{300} mΩ	1606	911	485	458		442	473	547
RRR	1,07	1,20	1,46	1,66		1,55	1,62	1,77
Tc K	-	< 8	< 10.2	< 10.4		< 9.8	< 10.4	11.5
ΔTc	-	-	0.5	0.2		0.24	0.2	0.6

5. Conclusions

The best of our TFTS- cosputtered film samples gave us a value of T_c = 15.9 and RRR = 12.3. An improvement in cosputtering of V_3Si films could be reached with a higher deposition temperature. Due to sensitivity to impurities and lattice order defects in the A15 structure, for sputtering whole cavities absolutely homogeneous films are a must. In addition the shape of a cavity is more complex and the surface to be coated at its equator increases with growing surface distance at the same time. These requirements present itself far-reaching possibilities for coming research.

6. References

1 Feynman, The Feynman lectures on Physics, vol. II, Addison Wesley Publishing Company, Reading, 1964

2 Piel, H.;in Cern Accelerator School: Superconductivity in Particle Accelerators, ed. S. Turner, p. 149 ff., Cern 89-04, 1989

3 Kammerling Onnes, H.; Comm. Phys. Lab., Univ. Leyden, 1911

4 Tesla Collaboration, Tesla Test Facility Linac Design Report Version 1, March 1995

5 Quinn, D. J.; a. Ittner, W. B.: J. Appl. Phys. 33, 748, 1962

6 Bednorz, J. G.; Mueller, K. A.; Z. Phys. B, 64, 189, 1986

7 Vladimir Z. Kresin, Stuart A. Wolf, Fundamentals of Superconductivity, Plenum Press, New York, 1990

8 Meissner, W.; Ochsenfeld, R.; Naturwiss., 21 (1933)

9 Barden, J.; Cooper, L. N.; Schrieffer, J. R.: Phys. Rev., 108, 1957, p. 1175

10 Padamsee, H.: CLNS 90-1004, Review Lecture presented at th 1989/1990 US Particle Accelerator School, Brookhaven National Lab., July 1989

11 Flükiger, R.: Concise Encyclopedia of Magnetic & Supercond. Materials, Jan Evetts, 1992 Pergamon Press Ltd.

12 Vonsovsky, S. V.; Izyumov, Yu. A.; Kurmaev, E. Z.: Superconductivity of transition metals, Springer Verlag 1977

13 Junod, A.; Staudemann, J. L.; Muller, J.; Spitzli, P.: J. Low Temp. Phys. 5, 25 1971

14 Moffat, W. G.:"Handbook of Binary Phase Diagramms", General Electric Co., Technology Marketing Operation, Schenectady, New York, 1976

15 Klabund, "Thin films from free atoms and particles", Academic Press, INC. 1979

16 Haefner, Ren A.: "Oberflächen und Dünnschichttechnik"", WFT Springer Verlag, 1987

17 Wehner, G. K.; Anderson, G.S.: Handbook of thin film technology, New York, Mc Graw-Hill 1970

18 Fetz, H.; Oechsner, H.: Compt. Rend. VI CIPIG, Paris, 1963, vol 2, p. 39

19 Almen, O.; Bruce, G.: Trans. 8th Nat. Vac. Symp. 1962, 245

20 Kaminsky, M.: Atomic and ionic impact phenomena on metal surfaces, Springer Verlag, Berlin 1965

21 Thornton, J. A.; Penfold, A. S.: Thin film processes, Academic Press 1978, II-2, p 82

22 Messier, A.; Gir, A. P.; Roy, R. A.: Revised structure zone model for thin film physical structure, J. Vac. Sci. Technol. A.2 (2) 1984 p. 500-503

23 Thornton, J. A.: The microstructure of sputter-deposited coatings, J. Vac. Sci. Technol. A.4(6) 1986 p. 3059-3065

24 Deposition technologies for thin films and coatings; Sputter deposition processes, p. 289

25 Fan, Qihua; Uniformity of target erosion and magnetic film ..., J. Vac. Sci. Technol. A 10(5), Sept/Oct 1992

26 Almedeida, J. B.: Design of magnetrons for sputtering, Vacuum/Vol.39/p. 720/1989

27 Pena, O.; An easy non-distructive inductive method to characterize superconducting materials with planar geometry

28 Testardi, L. R. et. al.: Preparation and analysis of superconducting Nb-Ge films, Phys. Lett. Rev. B Vol. 11, No. 11, 1975

29 Hardy, G. F.; Hulm, J. K.: The superconductivity of some metal compounds, Phys. Rev., Vol. 93, No. 5, p. 1004-1016, 1954

30 Moore, D. F.; Rowell, J. M.; Beasley, M. R.: Solid State Commun. 20, 305 (1976); D. F. Moore, thesis (Stanford University, 1978), (Ginzton Laboratory Report no. 2788); D. F. Moore, M. R. Beasley, and J. M. Rowell submitted to LT 15 Conference, Grenoble, France (unpublished)